Blukis, R., Schindler, M., Couasnon, T., Benning, L. G. (2022): Mechanism and Control of Saponite Synthesis from a Self-Assembling Nanocrystalline Precursor. - Langmuir, 38, 25, 7678-7688.

https://doi.org/10.1021/acs.langmuir.2c00425

Mechanism and control of saponite synthesis from a self-assembling nanocrystalline precursor

Roberts Blukis[1]*, *Maria Schindler*[1], *Thaïs Couasnon*[1], *Liane G. Benning*[1]

[1]German Research Center for Geosciences, GFZ, Telegrafenberg, 14473 Potsdam, Germany

Saponite, clay synthesis, aluminosilicates

ABSTRACT

Saponite is a smectite group clay mineral that finds applications in chemical industry as a catalyst or catalyst precursor as well as in nanocomposites used for structural or catalytic applications. Saponite of a controlled composition, crystallinity, particle size and morphology, would be highly beneficial to industry, however, such materials are not found in a sufficiently pure form in nature. Synthetic methods to produce saponite with specific properties are currently lacking as the understanding of the mechanisms controlling its formation, crystallinity, particle size and morphology, are limited. Understanding the saponite formation mechanism is crucial for the development of a highly-tuned and controlled synthesis leading to materials with specific properties. Here we report a new chemical reaction mechanism explaining the nucleation and kinetics of saponite growth at different pH, at 95-100 °C and under influence of pH modifying additives explored via a combination of X-ray scattering methods and infrared spectroscopy. Our results show that the main factor affecting the nucleation and growth kinetics of saponite is the

pH, which has a particularly significant impact on the rate of the initial nucleation. Non-uniform reactivity of the aluminosilicate gel also significantly affected saponite growth kinetics and caused a change in rate determining step as seen in graphical abstract. The most crystalline saponite was obtained when the nucleation was suppressed by a low initial pH (<7) but the reaction was performed at a higher pH of about 9. The stacking of the saponite sheets can be further improved by a separate post-synthesis treatment with an alkali (NaOH) solution. A method for synthesizing a high crystallinity saponite through a simple, ambient pressure method, that could easily be upscaled for industrial purposes.

1. INTRODUCTION

Clays are sheet silicates used in catalysis in the chemical industry or as nanocomposite components in manufacturing in addition to more traditional applications such as production of ceramics or building materials [1–5]. Currently almost all industrially consumed clays are mined or are derived from mined sources. However, natural clays often lack the high purity needed for specialized industrial processes[4]. In addition, the particle size of natural clays cannot be freely controlled, a feature that is of particular importance to nanocomposites as it affects the mechanical properties[6]. Development of synthetic methods capable of producing pure, high quality clay minerals with specified particle sizes is highly desirable for industrial catalytic and nanocomposite applications[2,3,7].

Clays consist of an octahedral layer of cations (usually M^{2+} or M^{3+}) coordinated by oxygen atoms and hydroxy groups (Figure S1), surrounded on both sides (in some clay minerals, like kaolinite, only on one side) by tetrahedrally coordinated silicon layers (solid solution with M^{3+} cations, such as Al^{3+} is possible) forming sheets, that are usually separated by hydrated metal ions. Among

clays, saponite, is of high relevance as it has important applications in a series of catalytic processes [2,5,7,8] , and has a structure that allows solid solutions to be formed in both, the tetrahedral and octahedral, layers. As such, saponite, belongs to the trioctahedral smectite group and contains mainly Mg^{2+} in the octahedral layer and a solid solution of Al^{3+} and Si^{4+} in the tetrahedral layer (model composition used in this study $Na_{1.2}(Al_{1.2}Si_{6.8})Mg_6)O_{20}(OH)_4 \cdot nH_2O$, Figure S1) with the charge balance provided by hydrated Na^+ or other interlayer ions[4]. There are various methods describing clay synthesis, including saponite[9,10], using either high pressure and high temperature hydrothermal conditions[8,11–13], very low concentrations and long reaction times[14,15] or ambient pressure and moderate temperature synthesis (<100 C°)[16–21]. However, all of these methods produce clays of much lower crystallinity than natural ones and the clay formation mechanism has never been accurately described[9].

Currently there are three main clay mineral formation mechanisms suggested: (a) rapid initial formation of nuclei that is followed by their coalescence into sheets[20,21], (b) self-assembly of aluminosilicate sheets in solution followed by attachment of octahedral layer cations, then followed by stacking[11] or (c) self-arrangement of the amorphous aluminosilicate gel starting material after it has been infused with Mg^{2+} ions[16].

Furthermore, many of the parameters that affect the nucleation and growth reactions, (e.g., pH [11] , organic additives [12,13,16]) are still poorly understood as is the saponite growth kinetics with even the reaction order not being clearly known[16,20,21]. Many studies have used organic additives in clay synthesis which often are carboxylates or nitrogen bases that are potential complexing ligands towards Mg^{2+} and Al^{3+} [12,13,16,19,22]. Yet their role in or influence on the clay formation processes have not been quantitatively assessed. Interestingly, various organic compounds have been postulated to have played a crucial role in the apparent changes in clay mineral abundance

throughout geological time[23,24] and have even been proposed to be the catalyst for the clay formation[22].

In this study we aimed to resolve some of the existing ambiguities and quantitatively assess the formation mechanism of saponite by monitoring the nucleation and crystallization of saponites with X-ray scattering methods and infrared spectroscopy (IR) analysis. In particular, we focused on the initial nucleation and growth and evaluated the effects of pH and various organic additives (Table 1, S1) on the nucleation and growth steps of the saponite formation process.

2. EXPERIMENTAL METHODS

2.1 Saponite synthesis

Saponite was synthesized following a slightly modified method from Besselink et al (2020)[16], the replicate of which is referred to as "Default conditions" (Table 1) with the other syntheses being derived from it by changing or removing the additives. The synthesis proceeded through 2 main steps described by the following equations:

Step 1: Synthesis of the aluminosilicate gel:

$$Na[Al(OH)_4]_{(aq)} + 6.8\ Na_2SiO_{3(aq)} + 4.4\ H_2O \rightarrow Na_{1.2}(Al_{1.2}Si_{6.8})O_{16(aq/s)} + 13.6\ NaOH_{(aq)}$$ eq (1)

The formation process and structure of the aluminosilicate gel is rather well understood and will not be discussed further [25–28].

Step 2: Saponite synthesis, the main focus of this study:

$$Na_{1.2}(Al_{1.2}Si_{6.8})O_{16(aq/s)} + 6\ MgCl_{2(aq)} + 12\ OH^-_{(aq)} \rightarrow Na_{1.2}([Al_{1.2}Si_{6.8}]Mg_6)O_{20}(OH)_{4(s)} + 12\ Cl^-_{(aq)}$$ eq (2)

In all experiments, the aluminosilicate gel was produced by mixing an alkaline sodium aluminate solution with a 1.2 M Na_2SiO_3 solution and heating the resulting suspension at 95 ºC for 1 hour under reflux (eq. 1).

The resulting strongly alkaline aluminosilicate gel was cooled to room temperature. A 0.21 M $MgCl_2$ solution containing various additives (Table 1, S1) was then added. The pH of the mixture was adjusted to the desired value (between pH = 7 and 11, Table 1) with 2 M HCl and the reaction mixture was heated to 95 ^{0}C and kept stirring for 72 hours (3 days) under reflux (eq. 2). For kinetic monitoring aliquots were taken and quenched in cold water after which the pH was recorded. The solid reaction products were separated by centrifugation and washed three times by resuspension in water followed by centrifugation (for full detailed experimental procedure see SI Section 1.2).

2.2 Saponite synthesis variations

Variations of the synthesis process were tested to explore the nucleation process of saponite (a) or to achieve a more crystalline saponite product (b and c).

(a) The solid and liquid components of the aluminosilicate gel (produced in step 1, eq. 1) were separated by centrifugation. The resulting liquid was rapidly mixed with the 0.21 M $MgCl_2$ solution, leading to an instantaneous formation of a white precipitate that was separated from the supernatant by filtration, washed on the filter with water and dried for 24 h in vacuum. The product of this reaction is hereafter referred to as "saponite precursor".

(b) Aluminosilicate gel synthesized as described above (step 1, eq. 1), was acidified to pH = 3 using 2 M HCl, (instead of the usual pH 7 - 11) and mixed with a solution containing $MgCl_2$ (0.21 M) and urea (0.84 M). After about 5 minutes the pH of this mixture was re-adjusted to pH = 7 using 1 M NaOH and the mixture heated at 95 ºC under reflux for 72 hours while stirring. The reaction products were processed as described above (Section 2.1) and are referred to hereafter as "highly crystalline saponite".

(c) One gram of dry 'highly crystalline saponite' produced in (b) was mixed with 20 mL 2.5 M NaOH solution and heated under reflux at 95 °C for 72 hours and under constant stirring. The

reaction products were processed as described above (Section 2.1) and the solids are referred to hereafter as "alkali treated saponite".

Table 1. Most significant saponite synthesis with their initial and final pH values as well as the relative crystallinity of the final products (for the full list of see Table S1).

Synthesis name	Additives (concentrations given relative to the total reaction volume)	Kinetics monitored	pH initial	pH final	Relative crystallinity
Saponite precursor	N/A	No	N/A	N/A	N/A
Highly crystalline saponite	N/A	No	See Section 2.2 (b)	8.58	2.61
Alkali-treated saponite	N/A	No	N/A	N/A	2.77
Default conditions[a] [16]	0.42 M urea; 0.105 M Imidazole hydrochloride	Yes	7.47	8.42	2.16
No additives pH 7	-	Yes	7.43	7.67	0.17
No additives pH 9	-	Yes	8.45	7.28	0.93
No additives pH 10	-	Yes	9.82	9.08	0.90
No additives pH 11	-	Yes	10.83	10.05	0.84
Urea pH 7	0.42 M urea	Yes	6.70	8.35	2.1
Urea pH 9	0.42 M urea	Yes	8.85	9.51	0.75
Differnet[b] additives pH 7	Different* additives, see Table S1	Selected reactions	6.52-7.69	5.97-7.42	0-0.25
Differnet[b] additives pH 9	Different* additives, see Table S1	Seleced reactions	8.67-9.00	7.46-9.00	0.51-1.6

[a] Synthesis procedure adopted from Besselink et al. (2020). [b] Results from use of different additives and concentrations are shown together here as it was shown that these additives have no significant effect on the synthesis (see results and supporting information)

2.3 Characterization methods

The reaction products were analyzed using X-ray scattering (diffraction and reduced pair distribution functions, G(r)) and infrared spectroscopy. Imaging with a transmission electron microscope (TEM) and elemental analysis using energy dispersive spectroscopy (EDS) was also performed.

2.3.1 X-ray scattering

X-ray diffraction measurements were performed with a STOE STADI P diffractometer with a Cu X-ray source fitted with a curved Ge (111) monochromator and a DECTRIS MYTHEN2 detector in a flat plate transmission geometry. Diffraction patterns were measured over the 2Θ range of 0 – 84 degrees, with the sample plate being rotated relative to 2Θ at a ratio of 1:2, with the data collection time of about 10 minutes per data point with a resolution of 0.015 degrees 2Θ.

The relative crystallinity of the samples (Table 1) was assessed using an empirical measure, calculated as the peak-to-trough ratio of the scattering peak at Q = 2.4 $Å^{-1}$ and the trough at Q = 2.3 $Å^{-1}$. The resulting relative crystallinity could take any value from 0 (saponite diffraction peak at 2.4 $Å^{-1}$ not discernible from background) to infinity (theoretically). Higher relative crystallinity values mean a higher degree of ordering in the saponite formed as well as higher saponite yield and lower amount of remaining aluminosilicate gel (starting material). Full details of the data processing and errors are given in the SI Section 4.

X-ray scattering patterns for the reduced pair-distribution function G(r) analysis were collected using a STOE STADI P diffractometer with an Ag X-ray source fitted with a curved Ge (111) monochromator and a DECTRIS MYTHEN2 detector in a Debye-Scherrer geometry, with the dry samples loaded into 0.5 mm diameter glass capillaries. Each sample was measured over ~5 days

across the Q range of 0 to 20.5 $Å^{-1}$, with a resolution of 0.015 degrees 2Θ and with longer measurement time devoted to the high Q region. The data analysis was performed using the PDFgetX2 package[29]. The raw scattering data was corrected for capillary and air scattering background, absorption, beam polarisation, sample geometry, Compton and multiple scattering. Lorch smoothing was applied to reduce termination ripples.

2.3.2 Infrared spectroscopy

Synthesis products were also analyzed using infrared absorption spectroscopy (IR) measured with a ThermoFisher Nicolet iS5 FT-IR spectrometer with KBr optics equipped with an iD7 single reflection diamond ATR accessory. For each sample, 32 spectra with a resolution of 4 cm^{-1}, were averaged. All band assignments and further details about peak assignment issues are described in the SI Section 2.6.

2.3.3 Conventional and cryo transmission electron microscopy (TEM)

Selected samples were imaged with a transmission electron microscope (FEI Tecnai™ G2 F20 X-Twin TEM) equipped with a field-emission gun electron source. TEM samples were prepared by suspending a few milligrams of the sample in 1-2 mL of acetone, ultrasonicating for 20 min, then drop-casting them onto holey carbon Cu TEM grids. The grids were then mounted on a Gatan double-tilt holder at room temperature or a Gatan double-tilt liquid nitrogen cryo-TEM holder at 77 K. Energy filtered images were acquired at an acceleration voltage of 200 kV on a Gatan GIF Tridiem detector.

2.3.4 Liquid-cell scanning transmission electron microscopy (LC-TEM)

Using the same TEM as described above LC-STEM was applied to assess the nature of saponite under hydrated conditions. Measurements were performed at an acceleration voltage of 200 kV

using liquid cells consisting of two silicon wafers (E-chips) assembled onto a sample holder (Protochips Inc., Poseidon 300). Imaging of the samples in their native hydrated conditions was performed in STEM mode using a high-angle annular dark-field detector (STEM-HAADF), with a 30 μm condenser aperture and a spot size to maintain a constant beam current of 3.19 nA. All the STEM-HAADF images were acquired in a 512 by 512 pixel format with a pixel dwell time of 10 μs to reach an electron flux of 23.46 e^{-} $Å^{-2}$ s^{-1}.

2.4 Thermodynamic modelling

Thermodynamic calculations were performed with Geochemist's Workbench Community Edition 15.0 software, implementing the thermo.tdat thermodynamic database for aqueous mineral and gas reactions[30].

3 RESULTS AND DISCUSSION

All saponite synthesis experiments resulted in solid products of variable relative crystallinities between 0 and 2.77 (Table 1, Table S1) with higher crystallinities generally being observed in samples associated with higher pH. During the 3-day synthesis, the pH generally dropped, sometimes by up to 1 unit, yet, no significant trend in pH or relative crystallinity with respect to the organic additives or their concentrations was observed (see Table 1, Table S1 and Figure S2 and S3). pH decrease during the reaction is expected as the net process of saponite formation consumes OH^{-} (Equation 2).

3.1 Comparison of the saponite precursor and highly crystalline saponite

The saponite precursor and the highly crystalline saponite represent the most extreme isolable endmembers of the reaction starting from the very first isolable solid to the most crystalline final

material respectively, excluding additional post-treatments. The X-ray diffraction and the G(r) data of the saponite precursor (Figure 1 A, B) indicates that despite the apparent instantaneous formation, the saponite precursor shares many features with the final highly crystalline saponite. This similarity is demonstrated by the coinciding diffraction peaks of the two phases in the XRD patterns (Figure 1 A). The peak positions in the G(r)s of both materials are also very similar (Figure 1 B). Nevertheless, the relative intensities of the G(r) correlation peaks are different in the two materials, especially the Mg-O and (Al,Si)-O correlations, suggesting the saponite precursor is more magnesium rich then the highly crystalline saponite as confirmed by TEM EDS (Figure S6). Saponite precursor G(r) peak intensities decay to noise levels over about 10-15 Å (equivalent to about two unit cells), meaning, the saponite precursor is only short range ordered[31]. While the correlation peak intensities in the highly crystalline saponite G(r) also decay rapidly in the first 15-20 Å, the decay rate above 15 Å significantly reduces indicating a significant long range order.

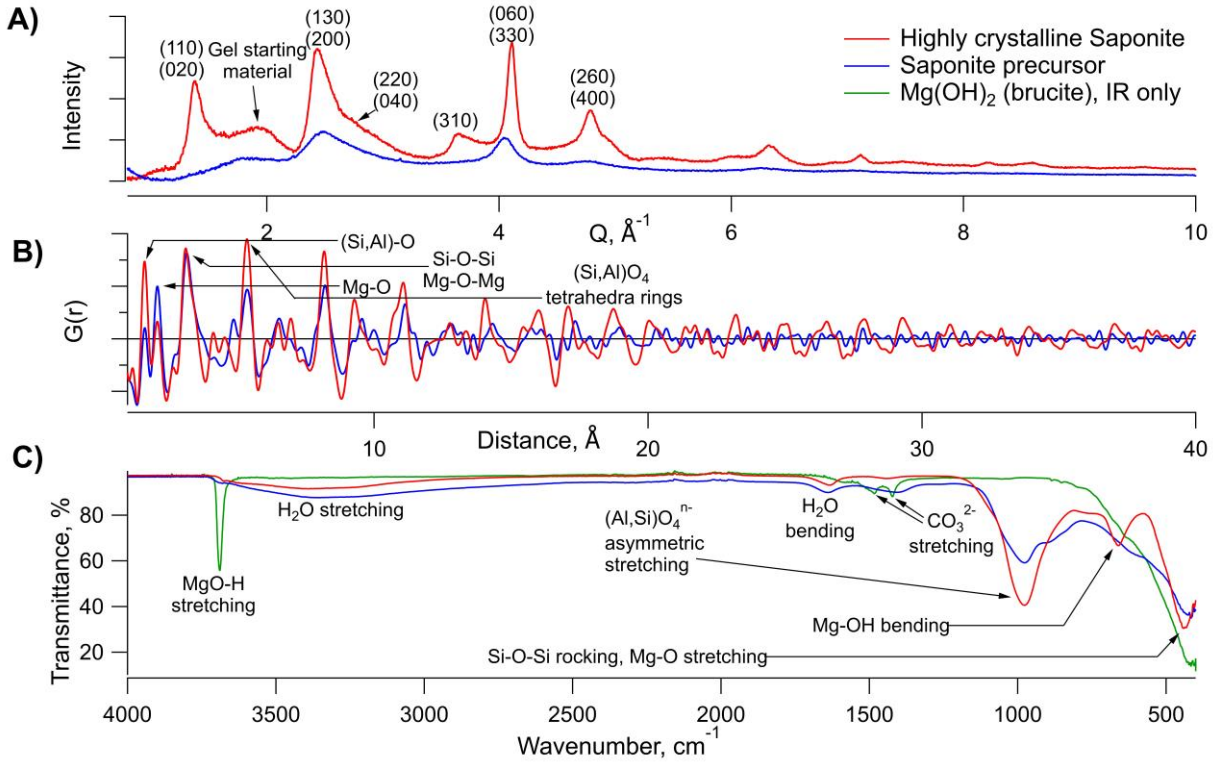

Figure 1. A) Ag-XRD patterns of the highly crystalline saponite (red) compared to the solid product obtained from the saponite precursor synthesis (blue). Note the very significant unreacted gel peak in the highly crystalline saponite pattern, which is less pronounced in the less crystalline saponite precursor. B) Reduced pair distribution functions G(r)s of the highly crystalline saponite (red) and the saponite precursor (blue). C) IR spectra of the highly crystalline saponite (red) and the saponite precursor (blue) as well as a spectrum of magnesium hydroxide ($Mg(OH)_2$, brucite, green) for comparison (brucite sample has a minor magnesite impurity indicated by carbonate absorption peaks near 1450 cm^{-1}.

Conventional and cryo-TEM imaging of the samples (Figure 2, S4) shows the highly crystalline saponite consists of ~ 400 nm to 1 μm diameter particles composed of aggregated stacks of 5 ± 2 sheets around 35 ± 5 nm in width (Figure 2). Liquid-cell TEM analyses of the highly crystalline saponite (Figure S5) confirms the heavily aggregated and entangled sheet-like nature of the material is an intrinsic material property and not an artefact. Although both, the XRD and G(r) (Figure 1 A, B), revealed the saponite precursor was short range ordered, it was impossible to obtain high-resolution images with the conventional or cryo-TEM due to the beam sensitivity of the sample making it appear amorphous. Selected area electron diffraction patterns were consistent with a very poorly crystalline material and showed features very similar to those observed with the XRD (Figure S4).

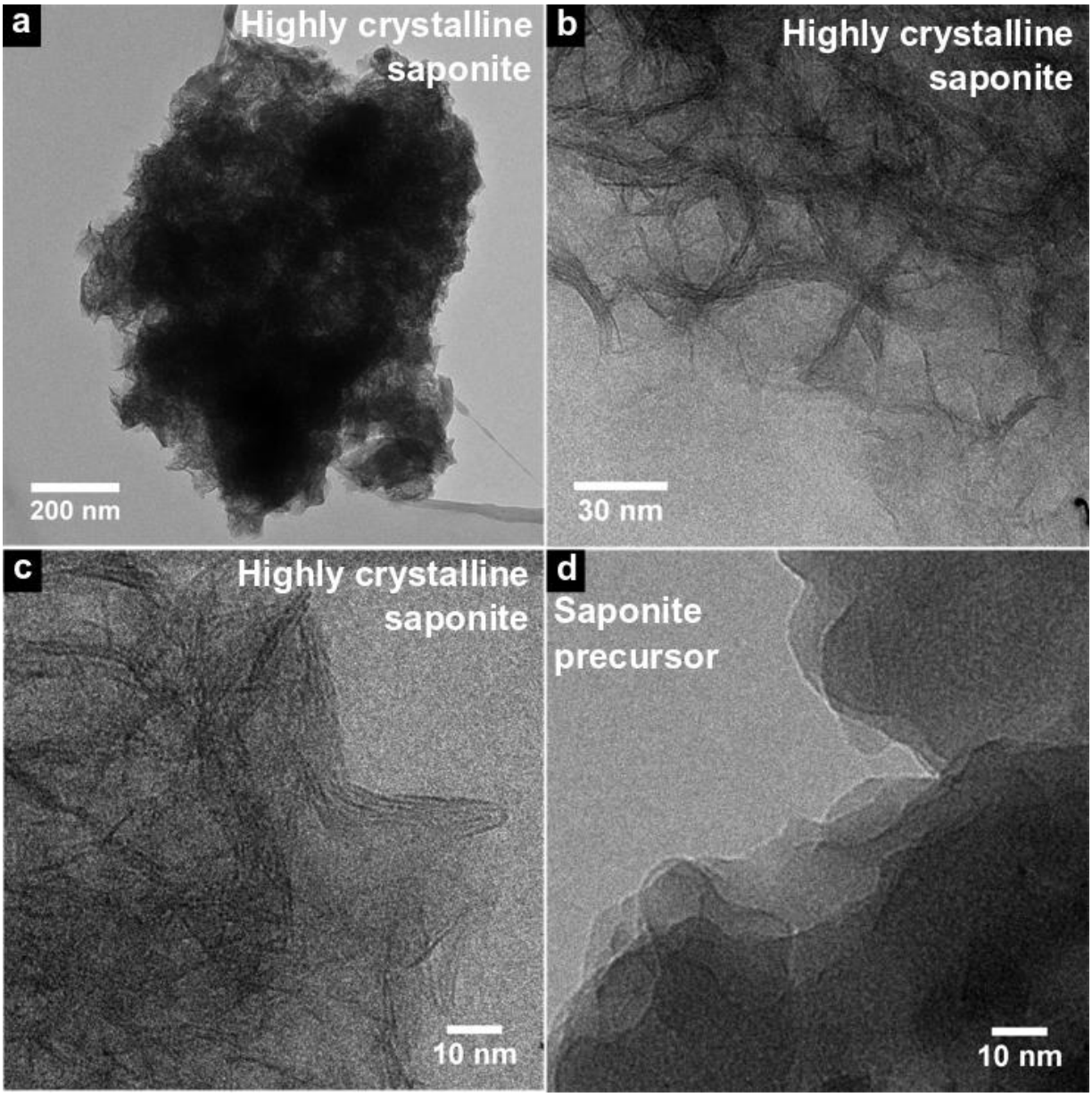

Figure 2. Conventional (a, b) and cryo-TEM (c) images of the highly crystalline saponite and cryo-TEM of the saponite precursor (d) show that the saponite precursor appears amorphous, while stacked and entangled sheets are visible in all images of the highly crystalline saponite.

To further evaluate the differences and similarities between the saponite precursor and the highly crystalline saponite, their IR spectra were compared (Figure 1 C). Both contain a small peak

corresponding to MgO-H stretching vibrations at 3690 cm^{-1}, and the water absorptions between 3600 and 3000 cm^{-1} (stretching) and at 1640 cm^{-1} (bending)[32]. Aluminosilicate component absorbs strongly in both materials in the range between 1200-800 cm^{-1}. However, only one peak in this region is clearly resolvable in the highly crystalline saponite, while in the saponite precursor the absorption band is composed of multiple overlapping peaks. This further confirms that, although the aluminosilicate component is present in both materials, the structures are not identical. The highly crystalline saponite is characterized by a well resolved Mg-OH bending mode band at 660 cm^{-1} while in the precursor this mode is either absent or shifted to ~ 620 cm^{-1}. There are also Si-O-Si bending mode absorption peaks in this region, therefore, this peak cannot be conclusively assigned[33,34]. However, the overall absorption in the 560-660 cm^{-1} region is significant in the saponite precursor spectrum indicating an intermediate stage between $Mg(OH)_2$ and the highly crystalline saponite. This is interpreted to be due to there being fewer $(Al,Si)O_4$ tetrahedra attached to the $Mg(OH)_2$ octahedral layers, which leads to the shift of the absorption peak maximum to lower wavenumber, closer to that of pure $Mg(OH)_2$. The attachment of the $(Al,Si)O_4$ tetrahedra is expected to be less ordered than in the highly crystalline saponite and the particle size of the saponite precursor is very small as shown by the G(r) (Figure 1 B). This results in the Mg-OH bending mode being very broad and shifted due to the multiple different local Mg-OH environments. Both materials also show a strong, broad absorption band at 420 cm^{-1}, where Mg-O and Si-O-Si bending modes are expected[34,35]. The similarities of MgO-H stretching peak at 3690 cm^{-1} and Mg-O stretching band at 420 cm^{-1} suggest that the magnesium environments are rather similar, although the Mg-O stretching band at 420 cm^{-1} overlaps with the Si-O-Si rocking mode, therefore the interpretation of this lower frequency band is inconclusive.

IR spectra of both, saponite precursor and highly crystalline saponite, show significant similarities to brucite, $Mg(OH)_2$, thereby implying significant structural similarities between the magnesium bonding environments in all three materials (Figure 1 C). However, despite the similarities in the magnesium bonding environments of these three materials the lack of brucite peaks in the XRD patterns (Figure 1 A) clearly show that brucite is not a byproduct of our saponite synthesis.

3.2 Saponite precursor nucleation

The significant similarities between the saponite precursor and the highly crystalline saponite observed in XRD, G(r)s and IR (Figure 1) indicate that many features of the highly crystalline saponite structure are already present in the initial saponite precursor precipitate. The nucleation is effectively instantaneous under the synthesis conditions used here. During the 72-hour reaction at 95 ºC, the unreacted reagents are converted into saponite, however, no fundamentally new structural motifs are formed. In this process saponite precursor develops a long range order, thereby becoming saponite. Its short range order is also refined to some extent as indicated by change in shape of the aluminosilicate asymmetric stretching band at ≈ 1000 cm^{-1} in the IR (Figure 1 C).

These results are consistent with the observations by Decarreau[20,36], who synthesized hectorite and stevensite, which are structurally very similar to saponite. Decarreau reported that reagent mixing produced a "precipitate containing only smectite nuclei" that were inferred to be crystalline based on TEM analyses[36]. However, Decarreau also used XRD to describe the clay nuclei as "pencil shaped" and by using the Scherrer equation he calculated these to be "stacks of 2-4 sheets along the c direction" as he also seems to have been unable to observe these features using HR-

TEM imaging. In the XRD pattern of our saponite precursor (Figure 1 A) this was not observed, as no (001) scattering peak was present. Therefore, significant stacking of sheets in the saponite precursor is not supported by our data. The geometry of the individual crystallites could not be evaluated using TEM due to beam sensitivity (Figure 2). Although no (001) scattering peak was observed in the XRD of the saponite precursor, the XRD data together with the TEM and IR data suggests the saponite precursor is very likely an equivalent material in the saponite system to the "clay nuclei" as reported Decarreau for the stevensite and hectorite system.

The saponite precursor was more Mg rich compared to the final saponite (EDS, Figure S6), therefore its most likely formation mechanism is the initial precipitation of individual octahedral layer fragments (brucite-like magnesium hydroxide sheets) of 10-15 Å in size. This step is immediately followed by the precipitation of aluminosilicate tetrahedra on their (001) surfaces. The rapid attachment of aluminosilicate tetrahedra leads to poor ordering reflected in very broad and poorly developed diffraction peaks in the XRD as well as a broader and more complex (Al,Si)-O asymmetric stretching band in the IR spectra (Figure 1 C). This formation pathway is consistent with the solubility calculations which show that during the mixing of aluminosilicate gel and Mg^{2+} solution the reaction mixture becomes oversaturated with respect to both, brucite and amorphous aluminosilicate gel, therefore both constituents are expected to precipitate (see SI Section S3.1).

The critical component to initiate the saponite precursor formation and ordering could be either the brucite-like $Mg(OH)_2$ sheets[14,22,37] or the aluminosilicate gel[11]. However, only the magnesium hydroxide sheets as the key initiator are consistent with our observations and the literature data, where it is well established that the precipitation of magnesium hydroxide by increasing pH leads to crystalline brucite[38] while the precipitation of aluminosilicates by lowering pH leads to an amorphous material[39]. Knight et al. (2007) identified nearly 50 silicate species (monomer, dimer

and many oligomers) in alkaline silicate solution, however, none of these where 6-membered rings or structurally similar species to motifs encountered in saponite structure that could directly participate in clay formation or templating without a significant geometry change[40]. The two most common fragments are monomeric and dimeric tetrahedra that are prime candidates for precipitation onto brucite-like magnesium hydroxide surface[14,22]. Therefore, the saponite nucleation process (formation of saponite precursor) could be approximated by the following two equations:

$Mg^{2+}_{(aq)} + 2OH^{-}_{(aq)} \rightarrow Mg(OH)_{2\,(s)}$

$Mg(OH)_{2\,(s)} + n\ Gel_{(aq)} \rightarrow Nuc_{(aq)}$

Where $Gel_{(aq)}$ represents the aluminosilicate gel ($Na_{1.2}(Al_{1.2}Si_{6.8})O_{16}$) and $Nuc_{(aq)}$ represents the saponite nuclei (saponite precursor).

It is important to note the saponite precursor was produced in the absence of any additives, demonstrating that no catalyst or template is required for saponite nucleation in contrast to the suggestions in other studies[22,24].

3.3 Highly crystalline saponite product

Guided by the present findings of the saponite nucleation, a method for producing highly crystalline saponite was devised. This was achieved by suppressing nucleation in the beginning of the reaction by mixing the aluminosilicate gel with magnesium chloride at low pH. Thereby the consumption of reagents during the instantaneous formation of a large number of nanocrystalline saponite nuclei was prevented. Instead, the slow increase in pH produced fewer nuclei allowing their growth to larger sizes. The product obtained displayed significant atom pair correlation peak intensities up to 40 Å in the G(r) (Figure 1 B), which was more than the saponite produced by Besselink et al. (2020), whose most crystalline product had atom pair correlation peaks only to 25

Å[16]. The pair correlation peaks of the highly crystalline saponite G(r) decay rather rapidly over the first 15-20 Å, however, the amplitude at r values above 20 Å stays approximately constant and significant. This indicates that the highly crystalline saponite sample was composed of two components - a poorly crystalline (short range ordered) material (rapid correlation peak decay over 15-20 Å) and a highly crystalline (long range ordered) material (slow correlation peak decay up to at least 40 Å). XRD data (Figure 1 A) indicates the highly crystalline saponite contains significant fraction of unreacted amorphous aluminosilicate gel (the poorly crystalline phase) in addition to crystalline saponite with clearly defined diffraction peaks (the highly crystalline phase). The G(r) peak decay rate of the poorly crystalline phase (15-20 Å) is similar to the peak decay rate of the saponite precursor, therefore this phase likely represents a material similar to saponite precursor prior to transformation into the highly crystalline saponite or a continuum of phases in between the fully amorphous aluminosilicate gel and the highly crystalline saponite (Figure S7).

3.4. Sheet stacking improvement with post-synthesis alkali treatment

To further increase the crystallinity of the saponite, a sample of highly crystalline saponite was treated with a 2.5 M NaOH solution (Section 2.2 (c)). The alkali treated saponite showed a very prominent (001) peak in the XRD pattern, not present in any other saponite synthesized here indicating significantly improved sheet stacking along (001) (Figure 3). In the highly crystalline saponite the (001) peak could be observed only as a slight shoulder on a large intensity increase towards very low Q values. A peak corresponding to (113) at Q ≈ 2 was also observed indicating improved layer stacking relative to one another. This is in contrast to many other synthetic clays where only (hk0) and (00l) peaks are observed[41,42]. The peaks in the XRD pattern of the alkali treated saponite are of a very similar broadness to those in the other saponites (Figure 3), indicating

that the defects present within the saponite sheets were not annealed and the sheet size was not changed by the reaction with OH^-. Furthermore, the asymmetric nature of the (110;020) and (130;200) peaks, which is very similar to those of the highly crystalline saponite, indicates that the turbostratic disorder has also not been significantly improved by the alkali treatment. The (113) peak is located in a region (Q = 1.5-3.4 $Å^{-1}$) of a rather elevated background, therefore it is very likely that unreacted gel is still present in the alkali treated saponite.

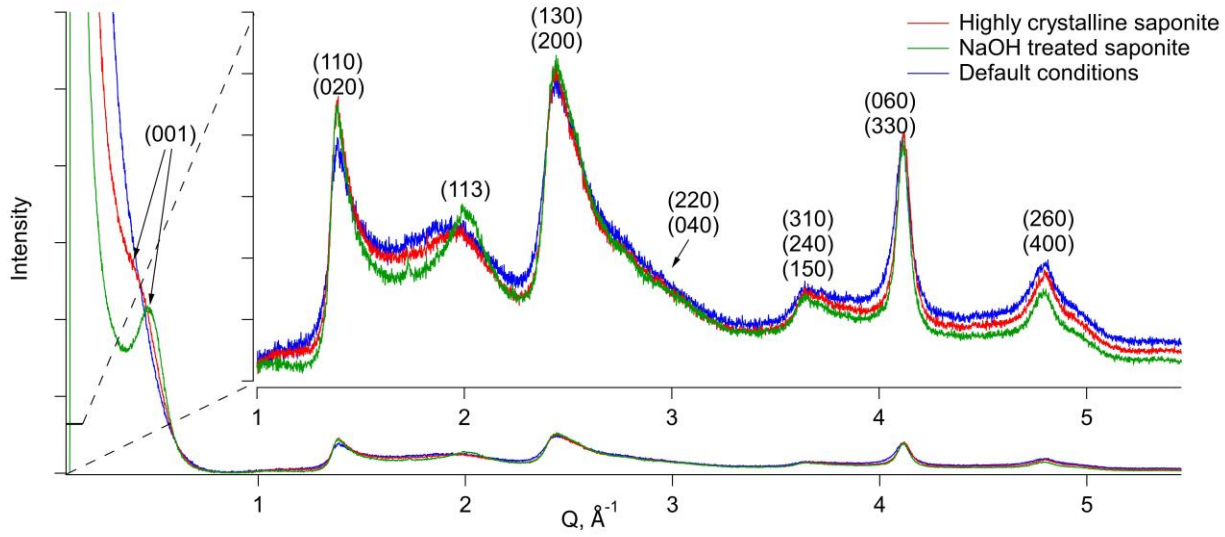

Figure 3. Cu-XRD patterns of saponite synthesized under "Default conditions" compared to the highly crystalline saponite and the alkali treated saponite (Table 1).

3.5 Saponite growth kinetics and pH dependence

XRD patterns of the time series of the saponite synthesis under the "Default conditions" (Figure 4 C), show a gradual development of diffraction peaks corresponding to saponite (with (110,020), (130,200) and (330,060) being the most prominent) as well as a slow decrease in intensity of the broad diffraction band representing the aluminosilicate gel starting material (1.4-2.3 $Å^{-1}$). The most significant changes happen within the first 24 hours of the reaction, with the saponite diffraction peak shape being only refined during the last 48 hours of the reaction. This is also reflected in the

relative crystallinity plot (Figure 4 A) where by far the biggest change in crystallinity occurs over the first 24 hours. The XRD patterns confirm the presence of a remnant aluminosilicate gel in the final product, but with a slightly narrower peak shape and position. These trends were also confirmed through the changes in the IR spectra (Figures S8, S9). pH changes during the reaction revealed that after starting the reaction at pH 7.47 at room temperature, the pH sharply increased to pH ≈ 8 and stabilized between pH 8 – 8.3 for the remainder of the reaction (Figure 4 B). This pH increase is caused by decomposition of urea at elevated temperature[43].

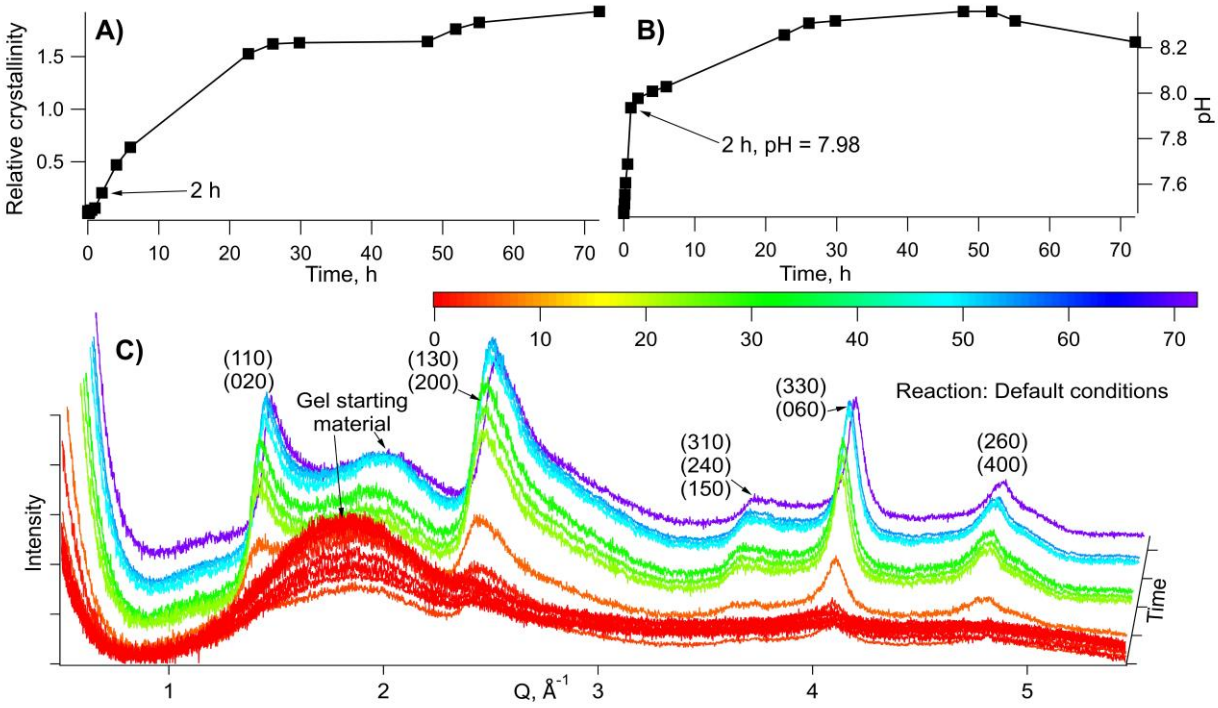

Figure 4. Time series of the changes in A) relative crystallinity and B) pH of the solid reaction products synthesized using the "Default conditions". The appearance of a significant relative crystallinity coincides with the pH reaching a value near 8 after two hours of heating at 95° C. C) Cu-XRD time series of the same reaction products. The final pattern (purple) corresponds to a reaction time of 72 hours (3 days).

The increase in relative crystallinity of saponites synthesized with no additives at different initial pH values (Figure 5) shows that higher initial pH, leads to faster development of crystallinity, which initially follow a non-linear trend that changes to a linear one. At a starting pH of 7 the initially formed solids were of very low relative crystallinity and even after 72 hours a relative crystallinity value of only about 0.2 was reached. In contrary at a higher initial pH of 9 the relative crystallinity increases very rapidly (during the first ≈10 minutes of heating the reaction) to values between 0.4 and 0.6 after which the increase in crystallinity is slower and linear with time. The rapid non-linear reaction progression followed by an approximately linear increase in relative crystallinity observed at pH 9 follows a very similar trend to that observed by Decarreau (1983) during the synthesis of stevensite and hectorite. At initial pH of 10 and 11 the initial rate of crystallinity increase is very high compared to pH 9, and largely takes place while the reaction is heated from room temperature to the reaction temperature (about 10 minutes). In the later part the pH 10 and 11 reactions, the crystallinity seemingly decreases. This matches with the observation that at high pH, the aluminosilicate gel peak appears to shift towards higher Q (Figure 4 C). This increases the scattering intensity in the trough between the (130,200) diffraction peak and the aluminosilicate gel peak and therefore reduces the calculated relative crystallinity (even though the saponite (130;200) peak remains unchanged), hence this decrease in relative crystallinity is an artefact.

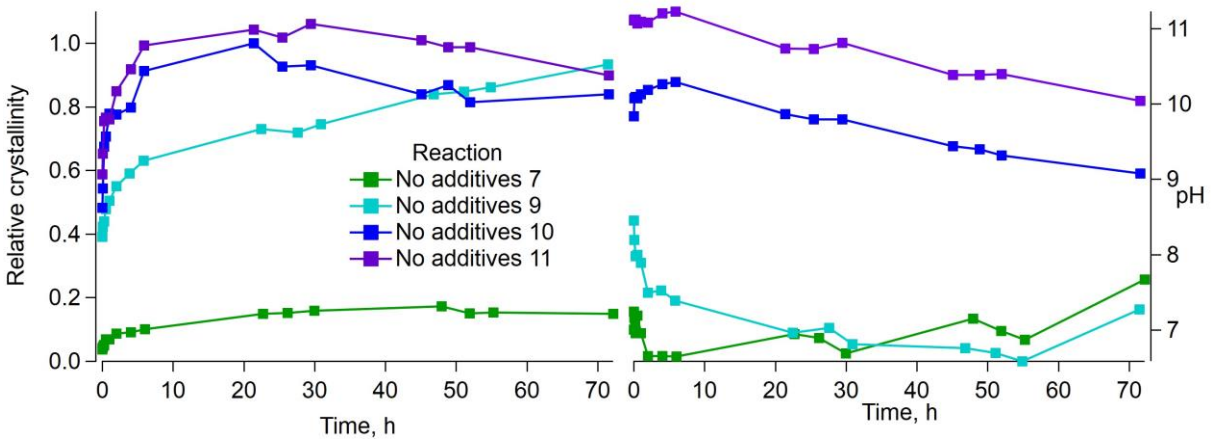

Figure 5. Increase in relative crystallinity of four "No Additive' experiment series at a different initial pH without further pH adjustment.

The relative crystallinity values of the saponite synthesis product with respect to the average pH (Figure 6, SI Section 1.3) revealed that for saponite to have a relative crystallinity above 0.5, the average reaction pH has to be about 8.5 or above ("No additives 9" is the only outlier) so that growth, not just nucleation, can occur. "No additives 9" is an outlier because most of the growth of this sample occurred in the very early stages of reaction when pH was higher (Figure 5). This is corroborated by the results from the experiments with an initial pH of 9 or above, which leads to rapid formation of many tiny nuclei in the very beginning of the reaction. All these nuclei competed for reagents for further growth, thereby limiting the relative crystallinity of the saponite product to about 1. The "No additives 9, 10 ,11" experiments also exemplify this as the relative crystallinity of the final products in these experiments was also about 1 regardless of the initial pH, as long as it was 9 or above. The highest relative crystallinity was observed when the initial reaction pH was about 7 but the average reaction pH was about 8.5. This condition was achieved by the addition of urea, however, urea by itself did not lead to high crystallinity saponite as the relative crystallinity was only 0.74, if the reaction was started at pH = 9 (Table 1).

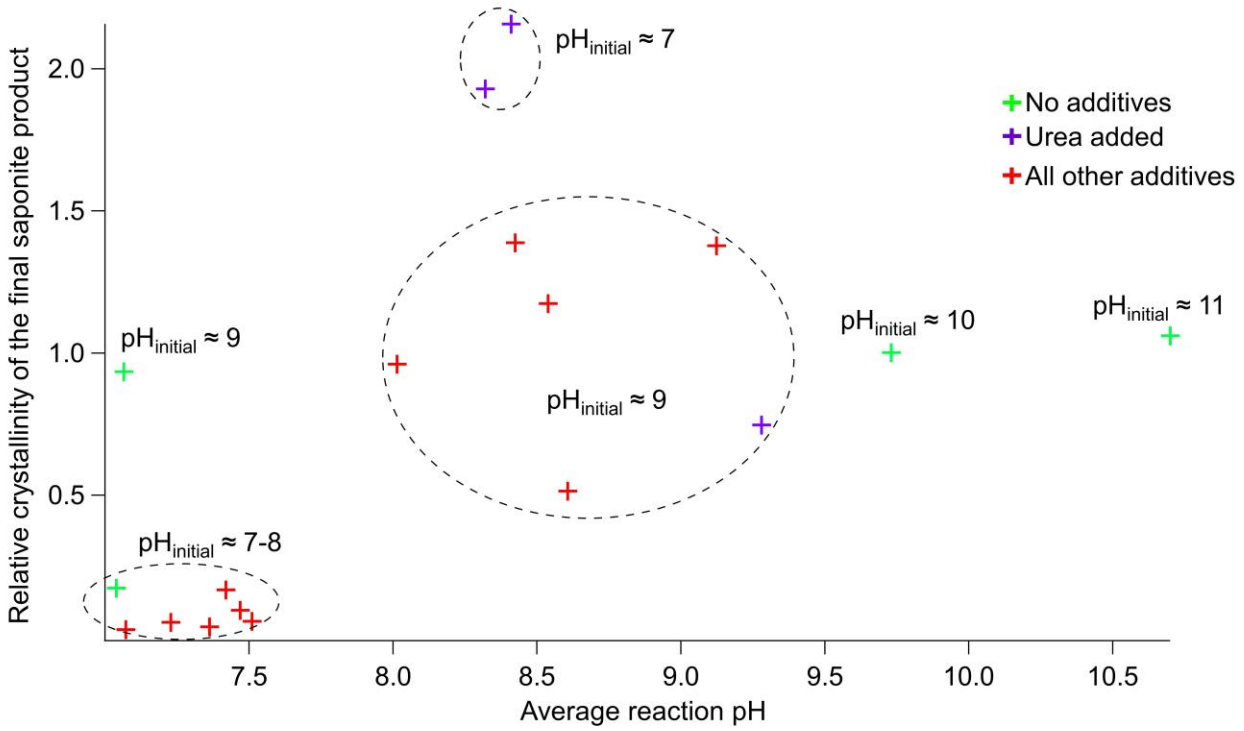

Figure 6. Relative crystallinity (determined from XRD data) of the final product (after 72-hour reaction) versus the average pH (see Section 2.3.1). The most crystalline saponite was obtained when the pH at the start of the reaction is near neutral, yet during the reaction it is higher, at about 8.5.

3.6 Saponite growth kinetics and modelling

In the additive free experiments (Figure 5), the initial growth of saponite was rapid with the increase in relative crystallinity following a profile of a 1st or higher order reaction in the first 10 hours after which the reaction proceeds via a linear 0th order process. The reaction progression was different in the "Default conditions" experiment where the reaction proceeded as a 1st order reaction, as shown before by Besselink et al. (2020). However, in the "Default conditions" experiment the rate determining factor was the decomposition of urea and not interactions between

the building blocks of saponite. Therefore, the additive free kinetics monitored experiments (Table 1) were used to develop a mechanism of saponite growth (SI Section 3.2).

The simplest model describing the observations was found to be a model consisting of two simultaneous processes was used (Figure 7, Table 2). Process one was set to produce saponite via 2^{nd} and process two via 0^{th} order kinetics. The two equations describing these model reactions and the resulting fitting parameters are shown below and in Table 2. Note, $Gel_{(inert)}$ was assumed to be of unlimited supply during the course of the reaction.

$2Gel_{(reactive)} \rightarrow$ Saponite k_2

$Gel_{(inert)} \rightarrow$ Saponite k_0

Within the context of the kinetics model the notations of $Gel_{(reactive)}$ and $Gel_{(inert)}$ are inferred to represent two components of the aluminosilicate gel starting material consisting of a dissolved or easily dissolvable (reactive) and solid (inert) components. Real amorphous aluminosilicate gel is expected to have a continuum of sites of different reactivities, however, here the two components representing the endmembers of reactivity were considered sufficient to explain the observed reaction progression. There is a general trend of $Gel_{(reactive)}$ and initial reaction rate increase with increasing pH, although these parameters seemingly decrease slightly as pH is increased from 10 to 11. This feature arises due to the reactions not being monitored from the beginning but from a more advanced stage where reaction at pH 11 has progressed more than that at pH 10 (Figure 5). It was also observed that prolonged treatment of the saponite at high pH results in a change of shape of the aluminosilicate peak and shifts it to the left thereby affecting the peak-to-trough ratio method used to evaluate relative crystallinity of the sample (Figures 3, S12).

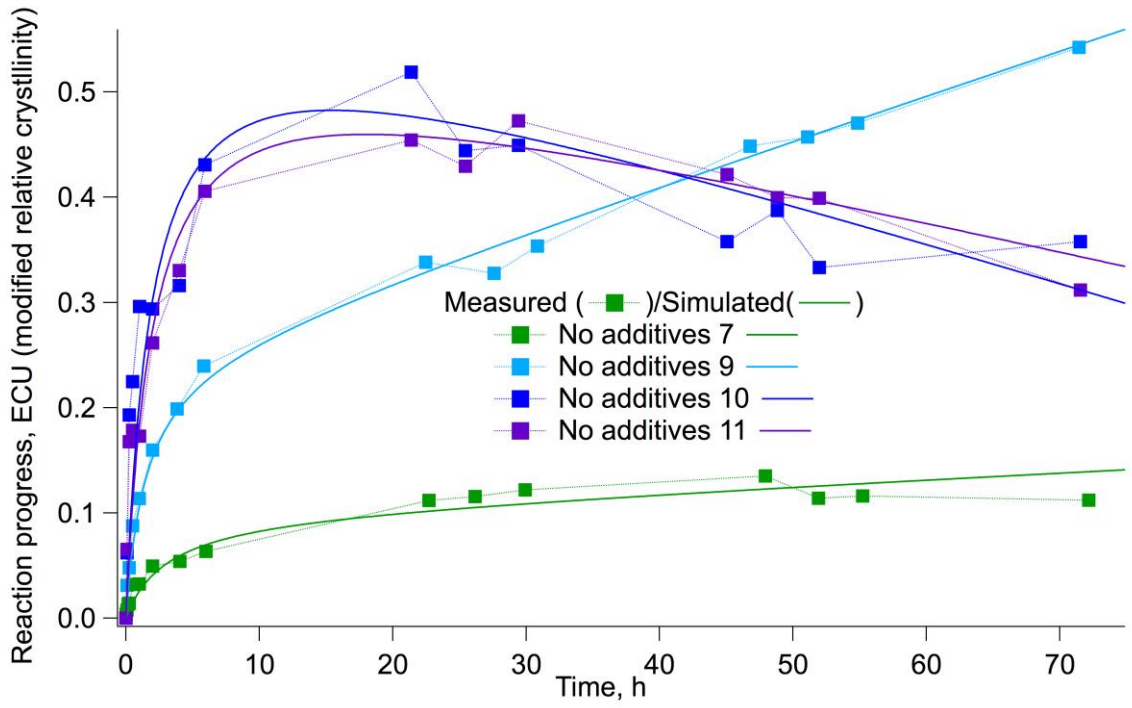

Figure 7. Kinetic model fits to the "No additives" experiments. The first relative crystallinity measurement was set as (0,0) point with respect to time and reaction progress.

Table 2. Kinetic modelling parameters fitted to the "No additives" experiment series (Table 1). Concentration is expressed as empirical concentration units (ECU). The error represents the difference between the experimentally measured and the simulated relative crystallinity.

Reaction	Initial pH	$[Gel_{(reactive)}]_{initial}$, ECU	K_2, h ECU^{-1} volume^{-2}	K_0, ECU h^{-1}	Initial reaction rate, ECU h^{-1}	Mean square error, ECU
No Additives 7	7.43	0.2	0.8	0.0006	0.032	0.011
No Additives 9	8.45	0.5	0.65	0.0042	0.163	0.013
No Additives 10	9.82	1.2	0.2	-0.0035	0.288	0.06

No Additives 11	10.83	1.15	0.2	-0.003	0.265	0.04

3.7 Saponite growth mechanism and nucleation and growth coupling

The kinetic data obtained together with other observations reported here and by previous authors allow a simple mechanism to be deduced that is consistent with all the experimental data.

The following observations have been considered:

- Saponite nucleation process is very rapid (Section 3.2)
- The reaction follows initially 2nd then 0th order kinetics with respect to saponite formation (Figure 7)
- Saponite growth proceeds faster at higher pH (Figures 5, 6)
- Alkali treatment does not significantly improve crystallinity of individual sheets (Figure 3)
- Incorporation of Mg^{2+} is not the rate determining step (RDS)[16]
- The final product is not concentration dependent (Figure S10).
- The aluminosilicate gel starting material has non-uniform reactivity[25–27,40,44,45]
- Additives have no effect on the reaction unless they change the pH (Tables 1, S1, Figures S2, S3)

Saponite growth is controlled by the aluminosilicate gel and can be understood as the following two-step process with a potentially reversible[25–27,40,44] gel dissolution step followed by an irreversible saponite growth step:

$Gel_{(s)} + OH^-_{(aq)} \rightarrow Gel_{(aq)} \rightarrow Saponite_{(s)}$

The gel dissolution step is supported by the positive dependence of the reaction rate on the pH (Figures 5, 6) in agreement with other studies on aluminosilicate gels[29–31,38,3]. It is also supported by the 0^{th} order reaction rate observable in the later stages of the reaction as the reagent is in a solid state.

The saponite growth step is supported by the initially observed 2^{nd} order reaction rate. Its irreversible nature is supported by the XRD data of the alkali treated saponite (Figure 3), where diffraction peaks of the highly crystalline saponite were not observed to improve in sharpness with alkali treatment.

Since magnesium is necessary but was shown not to be rate determining at the concentrations used here by low concentration experiments (SI Section 2.7) and by Besselink et al. (2020)[16] it is not included in the process describing saponite formation kinetics.

There is a change in the RDS of the saponite growth reaction, hence the 2^{nd} order rate profile changes to 0^{th} order one. This is due to exhaustion of the initially abundant dissolved $Gel_{(aq)}$ that is required in the 2^{nd} order step but is resupplied slowly by the 0^{th} order step. The main factor influencing the reaction rate is the pH. Higher pH generates higher concentrations of dissolved aluminosilicate gel $Gel_{(aq)}$ which is the rate limiting component of saponite growth. Furthermore, higher pH increases the nucleation rate due to the precipitation of magnesium hydroxide sheets, therefore generating more saponite nuclei that can participate in the second step.

The saponite growth step ($Gel_{(aq)} \rightarrow Saponite_{(s)}$) in itself can be expanded into the following possible reactions and elementary steps, where $Nuc_{(aq)}$ are saponite nuclei (saponite precursor), $Sap_{(s)}$ is saponite, $Gel_{(aq)}$ represents the dissolved aluminosilicate component (like $(Al,Si)O_4H_n^{-(4-n)}$, $Si_2O_7H_n^{-(6-n)}$ and similar[40]):

$$Nuc_{(aq)} + Nuc_{(aq)} \rightarrow Sap_{(s)}$$

$Gel_{(aq)} + Nuc_{(aq)} \rightarrow Sap_{(s)}$

$Nuc_{(aq)} + Sap_{(aq/s)} \rightarrow Sap_{(s)}$

$Gel_{(aq)} + Sap_{(s)} \rightarrow Sap_{/s)}$

$Sap_{(s)} + Sap_{(s)} \rightarrow Sap_{(/s)}$

The list is non-exhaustive due to the large number of different possible species that could be similar to any of the three constituents proposed here. Due to the very small size, saponite nuclei $Nuc_{(aq)}$, and potentially also small saponite particles $Sap_{(s)}$ behave like dissolved species and therefore follow 2nd order kinetics. The exact contribution of each reaction described above is impossible to quantify from the experimental data obtained so far, though all these processes are expected to contribute. The exact size at which, in terms of reaction kinetics, saponite starts behaving like a solid and not a dissolved species is also unknown.

The reaction mechanism proposed here is consistent with previously published observations of saponite, or similar smectite clay, synthesis, however, it does contradict interpretations of some of these studies (Table 3).

Table 3. Summary of the most detailed currently proposed mechanisms of saponite (or a very similar clay, stevensite) formation

Author/source	Mechanism summary	Problems
Decarreau[a] 1980,1983[20,21]	Rapid nuclei formation followed by the merger of the nuclei until the formation is complete	Does not explain the complex reaction rate with a change from 2nd to 0th order
Besselink et al. 2020[16]	1st order self-arrangement of the aluminosilicate gel after magnesium addition	Unreliable kinetics data due to interference from urea decomposition (see SI)
Vogels[b] at al. 1997[11]	Aluminosilicate sheet formation followed by the octahedral layer incorporation	Formation of aluminosilicate sheets before the octahedral layer is inconsistent with the

	followed by stacking of sheets	nucleation data presented here as well as known properties of aluminosilicate gels
This study	*Rapid nuclei formation initiated by magnesium hydroxide precipitation followed by OH^- catalysed growth.*	*Explains all available observations, although, some stages of the model have not been confirmed by direct observations*

[a] Data is for stevensite, not saponite, however, both share the same structure and have a very similar chemical composition. [b]Hydrothermal synthesis, therefore, alternative mechanisms are possible.

The saponite formation proceeds via process where nucleation and growth are coupled. To nucleate saponite precipitation of $Mg(OH)_2$ sheets are required, which is possible in a pH higher than 7.6 at 100 °C at the Mg^{2+} concentration used (SI Section 3.1). Higher pH will lead to higher nucleation rate due to increased precipitation $Mg(OH)_2$ as well as due to higher aluminosilicate $Gel_{(aq)}$ concentration in the solution. Therefore, new saponite nuclei forming later in the reaction can contribute to a distribution of sheet sizes as seen in TEM images (Figures 2 and S4), hence high rates of saponite nucleation are undesirable if large, uniformly sized sheets are to be formed. As shown above, to grow saponite sheets elevated pH of about 8.5 is desirable. This presents a problem as high pH promotes both, nucleation and growth, which together lead to the saponite product of small non-uniform size sheets of low crystallinity. Urea is a useful additive as reagents can be safely mixed at neutral or acidic pH initially leading to no reaction. However, thermal decomposition of urea increases pH gradually leading to a reduced nucleation rate, exemplified by the increased crystallinity of the highly crystalline saponite compared to the "Default conditions" or other synthesis modifications (Tables 1, S1). As shown by the conventional and liquid-cell TEM images as well as XRD data (Figure 2, 3, S5) highly crystalline saponite does not consist of

uniform, perfectly ordered and isolated sheets. Therefore, while an improvement, urea addition is not the perfect solution to the problem of nucleation and growth coupling. As the alkali treatment (Figure 3) shows, the stacking of the sheets can be improved post-synthesis, however, the crystallinity of individual sheets cannot, therefore high single sheet crystallinity has to be achieved in the initial synthesis step.

3.8 Proposed synthesis method for non-aggregated size-controlled large saponite sheets

An improved synthesis strategy to obtain size controlled and dispersed saponite can be suggested. Nucleation is the key control process, and should only happen in the beginning of the reaction. It should take place in a solution where both, Mg^{2+} and aluminosilicate component, are in a dissolved state with the nucleation initiating precipitation of magnesium hydroxide sheets. This can be achieved by a gradual increase in temperature (see SI Section 3.1). Dropwise addition of reagents creates high local concentrations for a very short time. Such local concentration variations can be sufficient to start an uncontrolled nucleation at the addition location. The further reaction should take place in a hot solution under atmospheric pressure at pH 9 with the aluminosilicate component (ideally dissolved) and Mg^{2+} solution being added very gradually to match the rate of the reaction and not to reach a concentration where $Mg(OH)_2$ would precipitate. The saponite synthesis discussed above was performed under conditions where the aluminosilicate component was rate limiting. However, if the reaction is performed at very low magnesium concentrations, magnesium becomes rate limiting. Under such conditions the attachment of new aluminosilicate species to the growing clay sheets could become reversible. In such a case, clay of higher degree of ordering in the aluminosilicate sheets could result. Due to the low concentrations in this synthesis method it is excepted the sheet stacking could be poor, however, this can be

improved by alkali treatment as shown above. These steps will lead to saponite sheets that are larger, less agglomerated and better stacked than has been possible with the methods used so far[9].

4 CONCLUSIONS

Saponite formation is highly dependent on the pH with OH^- being fundamental for both, the nucleation, as well as the growth. The optimal pH for growing the largest and most ordered sheets was found to be pH 9. The formation mechanism of saponite was found begin with a very rapid nucleation with growth following initially 2^{nd} order kinetics followed by a change in RDS to 0^{th} order process. Organic additives such as amino acids, carboxylates and amines have no significant effect on the saponite nucleation or growth or the crystallinity of the final product. The effect of urea is significant but indirect, as it gradually increases pH to 9 through decomposition, which helps to limit the nucleation while not hindering growth. The stacking of the saponite sheets along the (001) direction is significantly improved by a post-synthesis alkali treatment. Our findings provide a pathway towards more controllable clay synthesis methods, which in turn could help make synthetic clay minerals with tuned chemical (composition) and physical (particle size, crystallinity) properties more accessible for industrial applications.

ASSOCIATED CONTENT

Supporting_information.docx Additional experimental procedure details, supplemental results, including figures, as well as additional discussion of errors

AUTHOR INFORMATION

Corresponding Author

German Research Center for Geosciences, GFZ, 14473 Potsdam, roberts.blukis@gfz-potsdam.de

Author Contributions

RB and LGB designed the project, RB and MS performed the synthesis experiments and most analyses; TC led the TEM imaging and analysis and thermodynamic calculations. RB wrote the paper and all authors contributed guidance and edits to final manuscript preparation.

Funding Sources

We acknowledge the support of the Helmholtz Recruiting Initiative (grant no. I-044-16-01) to LGB that funded this study.

ACKNOWLEDGMENT

We thank our colleagues in the Interface Geochemistry section at GFZ Potsdam for their support, in particular we thank Vladimir Roddatis for assistance in cryo-TEM image acquisition.

5 REFERENCES

(1) Okada, A.; Usuki, A. Twenty Years of Polymer-Clay Nanocomposites. *Macromol. Mater. Eng.* **2006**, *291* (12), 1449–1476. https://doi.org/10.1002/mame.200600260.

(2) Lambert, J.; Poncelet, G. Acidity in Pillared Clays: Origin and Catalytic Manifestations. *Top. Catal.* **1997**, *4*, 43–56. https://doi.org/10.1023/A:1019175803068.

(3) Kloprogge, J. Pillared Clays : Preparation and Characterization of Clay Minerals and Aluminum-Based Pillaring Agents, Univeristy of Utrecht, 1992, Vol. 91.

(4) Bergaya, F.; Adams, J. M.; Aouad, A.; Beneke, K.; Berry, R. W.; Bish, D. L.; Barack, A.; Brigatti, M. F.; Carrado, K. A.; Carretero, M. I.; Churchman, G. J.; Cohaut, N.; Decarreau, A.; Dekani, I.; Droy-Lefaix, T. M.; Nahhal, Y. EL; Elsass, F.; Forano, C.; Galan, E.; Gates, W. P.; Gmira, A.; Gomes, C. S. F.; Harvey, C. C.; Heller-Kallai, L.; Hibino, T.; Johnston, C. T.; Komadel, P.; Kuhnel, R. A.; Lagaly, G.; Leroux, F.; LLewellyn, P. L.; Madejova, J.; Mandalia, T.; McCabe, R. W.; Michot, L. J.; Mishael, Y.; Murad, E.; Nir, S.; Ogawa, M.; Petit, S.; Polubesova, T.; Pusch, R.; Rabinovitz, O.; Rouquerol, F.; Rouquerol, J.; Rubin, B.; Ruiz-Hitzky, E.; Rytwo, G.; Sanz, J.; Schoonheydt, R. A.; Seyama, H.; Soma, M.; Srodon, J.; Stucki, J.; Tateo, F.; Taviot-Gueho, C.; Tazaki, K.; Tchoubar, D.; Theng, B. K. G.; Undabeytia, T.; Van Damme, H.; Van Meerbeek, A.; Vayer, M.; Villieras, F.; Yuan, G. *Handbook of Clay Science, Volume 1*, 1st ed.; Bergaya, F., Theng, B. K. G., Legaly, G., Eds.; Elsevier science, 2006.

(5) Zhou, C. H.; Zhou, Q.; Wu, Q. Q.; Petit, S.; Jiang, X. C.; Xia, S. T.; Li, C. S.; Yu, W. H. Modification, Hybridization and Applications of Saponite: An Overview. *Appl. Clay Sci.* **2019**, *168*, 136–154. https://doi.org/10.1016/j.clay.2018.11.002.

(6) Yousfi, M.; Livi, S.; Dumas, A.; Le Roux, C.; Crépin-Leblond, J.; Greenhill-Hooper, M.; Duchet-Rumeau, J. Use of New Synthetic Talc as Reinforcing Nanofillers for Polypropylene and Polyamide 6 Systems: Thermal and Mechanical Properties. *J. Colloid Interface Sci.* **2013**, *403*, 29–42. https://doi.org/10.1016/j.jcis.2013.04.019.

(7) Kloprogge, J. T. Synthesis of Smectites and Porous Pillared Clay Catalysts: A Review. *J. Porous Mater.* **1998**, *5* (1), 5–41. https://doi.org/10.1023/A:1009625913781.

(8) Bisio, C.; Gatti, G.; Boccaleri, E.; Marchese, L.; Superti, G. B.; Pastore, H. O.; Thommes, M.

Understanding Physico-Chemical Properties of Saponite Synthetic Clays. *Microporous Mesoporous Mater.* **2008**, *107* (1–2), 90–101. https://doi.org/10.1016/j.micromeso.2007.05.038.

(9) Kloprogge, J. T.; Komarneni, S.; Amonette, J. E. Synthesis of Smectite Clay Minerals: A Critical Review. *Clays Clay Miner.* **1999**, *47* (5), 529–554. https://doi.org/10.1346/CCMN.1999.0470501.

(10) Ponce, C. P.; Kloprogge, J. T. Urea-Assisted Synthesis and Characterization of Saponite with Different Octahedral (Mg, Zn, Ni, Co) and Tetrahedral Metals (Al, Ga, B), a Review. *Life* **2020**, *10* (9), 1–32. https://doi.org/10.3390/life10090168.

(11) Vogels, M. J.; Breukelaar, I. J.; Kloprogge, J. T.; Jansen, J. B. H.; Geus, J. W. Hydrothermal Crystallization of Ammonium-Saponite at 200 ° C and Autogeneous Water Pressure. *Clays Clay Miner.* **1997**, *45* (I), 1–7.

(12) Carrado, K. A.; Thiyagarajan, P.; Song, K. A Study of Organo-Hectorite Clay Crystallization. *Clay Miner.* **1997**, *32* (1), 29–40. https://doi.org/10.1180/claymin.1997.032.1.05.

(13) Carrado, K. A. Preparation of Hectorite Clays Utilizing Organic and Organometallic Complexes during Hydrothermal Crystallization. *Ind. Eng. Chem. Res.* **1992**, *31* (7), 1654–1659. https://doi.org/10.1021/ie00007a011.

(14) Harder, H. The Role of Magnesium in the Formation of Smectite Minerals. *Chem. Geol.* **1972**, *10* (1), 31–39. https://doi.org/10.1016/0009-2541(72)90075-7.

(15) Harder, H. Clay Mineral Formation under Lateritic Weathering Conditions. *Clay Miner.*

1977, *12* (4), 281–288. https://doi.org/10.1180/claymin.1977.012.4.01.

(16) Besselink, R.; Stawski, T. M.; Freeman, H. M.; Hövelmann, J.; Tobler, D. J.; Benning, L. G. Mechanism of Saponite Crystallization from a Rapidly Formed Amorphous Intermediate. *Cryst. Growth Des.* **2020**, *20*, 3365–3373. https://doi.org/10.1021/acs.cgd.0c00151.

(17) Vogels, R. J. M. J.; Kloprogge, J. T.; Geus, J. W. Synthesis and Characterization of Saponite Clays. *Am. Mineral.* **2005**, *90* (5–6), 931–944. https://doi.org/10.2138/am.2005.1616.

(18) Farmer, V. C.; McHardy, W. J.; Elsass, F.; M, R. hk-ORDERING IN ALUMINOUS NONTRONITE AND SAPONITE SYNTHESIZED NEAR 90 ° C : EFFECTS OF SYNTHESIS CONDITIONS ON NONTRONITE COMPOSITION AND ORDERING. *Clays Clay Miner.* **1994**, *42* (2), 180–186.

(19) Farmer, V. C.; Krishnamurti, G. S. R.; Huang, P. M. SYNTHETIC ALLOPHANE AND LAYER-SILICATE FORMATION IN Si02-A1203-FeO-Fe203-MgO-H20 SYSTEMS AT 23 ° C AND 89 ° C IN A CALCAREOUS ENVIRONMENT. *Clays Clay Miner.* **1991**, *39* (6), 561–570.

(20) Decarreau, A. Cristallogenèse Expérimentale Des Smectites Magnésiennes : Hectorite, Stévensite. *Bull. Minéralogie* **1980**, *103* (6), 579–590. https://doi.org/10.3406/bulmi.1980.7423.

(21) Decarreau, A. Etude Expérimentale de La Cristallogenèse Des Smectites. Mesures Des Coefficients de Partage Smectite Trioctaédrique - Solution Aqueuse Pour Les Métaux M2+ de La Première Série de Transition. *Sci. Géologiques, Bull. mémoires* **1983**, *74* (1), 17–23.

(22) Schumann, D.; Hartman, H.; Eberl, D. D.; Sears, S. K.; Hesse, R.; Vali, H. Formation of Replicating Saponite from a Gel in the Presence of Oxalate: Implications for the Formation

of Clay Minerals in Carbonaceous Chondrites and the Origin of Life. *Astrobiology* **2012**, *12* (6), 549–561. https://doi.org/10.1089/ast.2011.0635.

(23) Hazen, R. M.; Papineau, D.; Bleeker, W.; Downs, R. T.; Ferry, J. M.; McCoy, T. J.; Sverjensky, D. A.; Yang, H. Mineral Evolution. *Am. Mineral.* **2008**, *93* (11–12), 1693–1720. https://doi.org/10.2138/am.2008.2955.

(24) Hazen, R. M.; Sverjensky, D. A.; Azzolini, D.; Bish, D. L.; Elmore, S. C.; Hinnov, L.; Milliken, R. E. Clay Mineral Evolution. *Am. Mineral.* **2013**, *98* (11–12), 2007–2029. https://doi.org/10.2138/am.2013.4425.

(25) Dent Glasser, L. S.; Lachowski, E. E. Silicate Species in Solution. Part 1. Experimental Observations. *Dalt. Trans.* **1980**, 393–398.

(26) Lesley, B.; Glasser, S. D.; Lachowski, E. E. Silicate Species in Solution. Part 2. The Structure of Polymeric Species. *Dalt. Trans.* **1980**, 399–402.

(27) Harvey, G.; Dent Glasser, L. S. Structure and Properties of Aluminosilicate Solutions and Gels. In *Zeolite synthesis*; 1989; pp 49–65. https://doi.org/10.1021/bk-1989-0398.ch004.

(28) Huang, C.; Cormack, A. N. The Structure of Sodium Silicate Glass. *J. Chem. Phys.* **1990**, *93* (11), 8180–8186. https://doi.org/10.1063/1.459296.

(29) Qiu, X.; Thompson, J. W.; Billinge, S. J. L. PDFgetX2: A GUI-Driven Program to Obtain the Pair Distribution Function from X-Ray Powder Diffraction Data. *J. Appl. Crystallogr.* **2004**, *37* (4), 678. https://doi.org/10.1107/S0021889804011744.

(30) Bethke, C. M. *Geochemical and Biogeochemical Reaction Modeling*, 2nd ed.; Cambridge University Press: Cambridge, 2010.

(31) Egami, T.; Billinge, S. J. L. *Underneath the Bragg Peaks Structural Analysis of Complex Materials*, 1st ed.; Pergamon, 2003.

(32) Cai, J.; Du, J.; Chen, Z.; Lei, T.; Zhu, X. Hydrothermal Experiments Reveal the Influence of Organic Matter on Smectite Illitization. *Clays Clay Miner.* **2018**, *66* (1), 28–42. https://doi.org/10.1346/CCMN.2017.064084.

(33) Taylor, W. R. Application of Infrared Spectroscopy to Studies of Silicate Glass Structure: Examples from the Melilite Glasses and the Systems Na2O-SiO2 and Na2O-Al2O3-SiO2. *Proc. Indian Acad. Sci. - Earth Planet. Sci.* **1990**, *99* (1), 99–117. https://doi.org/10.1007/BF02871899.

(34) Galeener, F. L. Band Limits and the Vibrational Spectra of Tetrahedral Glasses. *Phys. Rev. B* **1979**, *19* (8), 4292–4297. https://doi.org/10.1103/PhysRevB.19.4292.

(35) Frost, R. L.; Kloprogge, J. T. Infrared Emission Spectroscopic Study of Brucite. *Spectrochim. Acta - Part A Mol. Biomol. Spectrosc.* **1999**, *55* (11), 2195–2205. https://doi.org/10.1016/S1386-1425(99)00016-5.

(36) Decarreau, A. Partitioning of Divalent Transition Elements between Octahedral Sheets of Trioctahedral Smectites and Water. *Geochim. Cosmochim. Acta* **1985**, *49* (7), 1537–1544. https://doi.org/10.1016/0016-7037(85)90258-3.

(37) Zhang, D.; Zhou, C. H.; Lin, C. X.; Tong, D. S.; Yu, W. H. Synthesis of Clay Minerals. *Appl. Clay*

Sci. **2010**, *50* (1), 1–11. https://doi.org/10.1016/j.clay.2010.06.019.

(38) Pokrovsky, O. S.; Schott, J. Experimental Study of Brucite Dissolution and Precipitation in Aqueous Solutions: Surface Speciation and Chemical Affinity Control. *Geochim. Cosmochim. Acta* **2004**, *68* (1), 31–45. https://doi.org/10.1016/S0016-7037(03)00238-2.

(39) Fernández-Jiménez, A.; Vallepu, R.; Terai, T.; Palomo, A.; Ikeda, K. Synthesis and Thermal Behavior of Different Aluminosilicate Gels. *J. Non. Cryst. Solids* **2006**, *352* (21–22), 2061–2066. https://doi.org/10.1016/j.jnoncrysol.2006.03.037.

(40) Knight, C. T. G.; Balec, R. J.; Kinrade, S. D. The Structure of Silicate Anions in Aqueous Alkaline Solutions. *Angew. Chemie* **2007**, *119* (43), 8296–8300. https://doi.org/10.1002/ange.200702986.

(41) Rits, V. A. D.; Plançon, A.; Sakharov, B. A.; Besson, G.; Tsipursky, S. I.; Tchoubar, C. Diffraction Effects Calculated for Structural Models of K-Saturated Montmorillonite Containing Different Types of Defects. *Clay Miner.* **1984**, *19* (4), 541–561.

(42) Viani, A.; Gualtieri, A. F.; Artioli, G. The Nature of Disorder in Montmorillonite by Simulation of X-Ray Powder Patterns. *Am. Mineral.* **2002**, *87* (7), 966–975. https://doi.org/10.2138/am-2002-0720.

(43) Shaw, W. H. R.; Bordeaux, J. J. The Decomposition of Urea in Aqueous Media. *J. Am. Chem. Soc.* **1955**, *77* (18), 4729–4733. https://doi.org/10.1021/ja01623a011.

(44) Krznarić, I.; Antonić, T.; Subotic, B. Physical Chemistry of Aluminosilicate Gels. Part 1. Influence of Batch Concentration on Chemical Composition of the Gels. *Zeolites* **1997**, *19*

(1), 29–40. https://doi.org/10.1016/S0144-2449(97)00049-3.

(45) Roelofs, F.; Vogelsberger, W. Dissolution Kinetics of Synthetic Amorphous Silica in Biological-like Media and Its Theoretical Description. *J. Phys. Chem. B* **2004**, *108* (31), 11308–11316. https://doi.org/10.1021/jp048767r.

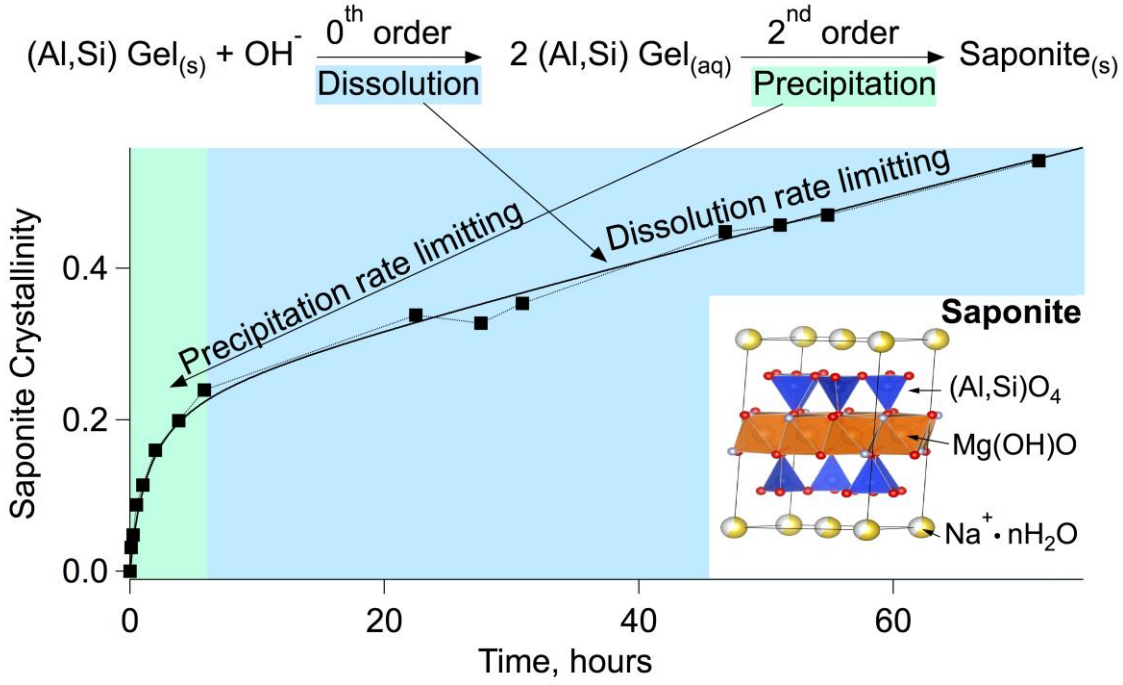

Table of contents graphic (graphic abstract)

Mechanism and control of saponite synthesis from a self-assembling nanocrystalline precursor

Roberts Blukis[1], Maria Schindler[1], Thaïs Couasnon[1], Liane G. Benning[1]*

[1]German Research Center for Geosciences, GFZ, Telegrafenberg, 14473 Potsdam, Germany

S 1. Experimental details

S 1.1 Reagents and glassware used

All reagents used were of 98% or higher purity and were used as received. All solid reagents were tested with XRD and/or IR and no significant impurities were detected. NaOH was determined to be 96% pure by HCl titration. Water used for solutions and synthesis was purified by reverse osmosis to resistivity of 18.2 MΩ cm^{-1} at 20 °C.

All synthesis procedures were performed in borosilicate round bottom flasks with two exceptions: Sodium aluminate was prepared in a polypropylene beaker and synthesis of alkali treated saponite (Section 2.2 (c) main text) was performed in perfluoroalkoxy alkane (PFA) flask. All solutions were prepared and stored in glass volumetric flasks with the exception of the 5 M NaOH and 1.2 M Na_2SiO_3 solutions that were prepared and stored in polypropylene flasks due to their high alkalinity. Stirring for the heating steps was provided by a combination of teflon coated magnetic stirring bars and a magnetic stirrer/hotplate in an oil bath. The exception was the synthesis of the alkali treated saponite, in which an

overhead stirrer with a teflon stirring shaft was used due to the poor wear resistance of the PFA flask material. Any dropwise additions were performed at a rate of about 1-2 droplets per second using a standard polyethylene Pasteur pipette (alkaline solutions) or glass Pasteur pipettes (all other solutions). During saponite synthesis, temperature was monitored directly in the reaction mixture (see below S 1.2 step 2). Due to the corrosive environment during the aluminosilicate gel synthesis (see below S 1.2 step 1) only the oil heating bath temperature was monitored. Time to heat the reactions from room (22 °C) to reaction (95-100 °C) temperature was about 10 minutes. pH of the reactions was measured using a SenTix 62 pH electrode, calibrated using Hamilton DuraCal pH standards. All centrifugation steps were performed by spinning the samples at 9000 revolutions per minute (7690 g_0) for 5 minutes in polypropylene centrifugation tubes.

S 1.2 Detailed experimental procedure

Step 1: Aluminosilicate gel synthesis

Aqueous solutions of sodium hydroxide (12.6 mmol, 2.52 mL, 5 M) and aluminium chloride (2.52 mmol, 2.52 mL, 1 M) were mixed until the initially formed white precipitate was dissolved. The resulting solution was added dropwise to a sodium silicate solution (14.3 mmol, 11.9 mL, 1.2 M), while stirring rapidly. The resulting suspension was heated at 100 ^{o}C for 1h under reflux, followed by the addition of water (43 mL) and cooling to room temperature. The resulting suspension was termed “aluminosilicate gel” and was used in the next step without isolation.

Step 2: Saponite synthesis

A magnesium chloride (12.6 mmol, 60 mL, 0.21 M) solution (pH ≈ 6) containing no or specific additives (full details in Table S1), was added to the aluminosilicate gel suspension dropwise, while stirring. The pH of the reaction mixture was then adjusted to the desired value (initial pH

of the mixture was ≈11.8 and was reduced to between pH 7 and 11; see pH initial, Table S1) with 2 M HCl. The resulting mixture was heated to 95 ^{o}C and stirred at 95 ^{o}C for 72 hours (3 days) under reflux. Time at which the reaction temperature of 95 ^{o}C was reached was considered the beginning of the reaction. The solid reaction products were separated by centrifugation and washed with water (3 x 60 mL) by resuspension followed by centrifugation. For reaction kinetic monitoring (see "Kinetics monitored" Table S1), 6 mL aliquots of the solution were taken from the reaction mixture, quenched in cold water (25 mL), the pH measured, and the solid reaction products separated by centrifugation and washed with water (3 x 25 mL) by resuspension followed by centrifugation. The obtained white pastes were dried in vacuum for 24 h (verified by IR). The resulting white material was ground in a powder in an agate mortar for further analysis (IR, XRD, TEM).

S 1.3 pH monitoring and calculations

Initial reaction pH was measured after mixing of all reagents but before heating to 95 °C (pH initial), as well as after completion of the reaction and cooling it to room temperature (pH final). The pH of all aliquots was measured after quenching. For kinetic (time) monitored reactions an average reaction pH was calculated as an empirical measure of OH^- concentration during the reaction. To do this, the measured pH was converted to $[OH^-]$, the area under the $[OH^-]$ versus time curve was integrated and the integral value was divided by time and converted back to pH. As the $[OH^-]$ changes over time were not linear, the average pH is an empirical measure of $[OH^-]$ during the reaction and cannot be used directly to calculate reaction rates.

Table S1. Full list of reactions performed in this study, excluding the low concentration experiments.

Synthesis name	Additives (concentrations given relative to the total reaction volume)	Kinetics monitored	pH initial	pH final	Relative crystallinity
Saponite precursor		No	N/A	N/A	N/A
Highly crystalline saponite		No	≈3, then 7	8.58	2.61
Alkali-treated saponite		No	N/A	N/A	2.77
Default conditions[a 1]	0.42 M urea; 0.105 M Imidazole hydrochloride	Yes	7.47	8.42	1.93
Default conditions[a] 2	0.42 M urea; 0.105 M Imidazole hydrochloride	No	6.74	8.36	2.13
No additives pH 7	-	Yes	7.43	7.67	0.17
No additives pH 7 2nd	-	No	7.52	6.70	0.29
No additives pH 8	-	No	8.09	7.40	0.71
No additives pH 9	-	Yes	8.45	7.28	0.93
No additives pH 10	-	Yes	9.82	9.08	0.90
No additives pH 11	-	Yes	10.83	10.05	0.84
Urea pH 7	0.42 M urea	Yes	6.70	8.35	2.1
Urea pH 9	0.42 M urea	Yes	8.85	9.51	0.75

Acetate pH 7	0.105 M sodium acetate	No	6.83	5.97	0.036
Acetate pH 9	0.105 M sodium acetate	No	8.88	7.72	1.6
Oxalate pH 7	0.105 M sodium oxalate	No	6.71	6.75	0.0
Oxalate pH 9	0.105 M sodium oxalate	No	8.87	8.1	1.0
Bicarbonate pH 7	0.105 M sodium bicarbonate	No	6.52	6.75	0.11
Bicarbonate pH 9	0.105 M sodium bicarbonate	No	8.81	8.13	1.2
Histidine pH 7	0.105 M histidine hydrochloride	No	6.82	7.19	0.025
Histidine pH 9	0.105 M histidine hydrochloride	No	8.80	8.23	1.0
DABCO pH 7	0.105 M DABCO	Yes	6.77	6.95	0
DABCO pH 9	0.105 M DABCO	Yes	8.91	8.33	1.4
En 7	0.105 M Ethylenediamine	Yes	6.84	7.42	0.094
En 9	0.105 M Ethylenediamine	Yes	8.96	9.00	1.4
Ammonia 7H	0. 525 M Ammonium chloride	Yes	6.85	7.15	0.021
Ammonia 9H	0. 525 M Ammonium chloride	Yes	8.87	8.36	1.2
Ammonia 7L	0.105 M Ammonium chloride	Yes	6.78	7.34	0
Ammonia 9L	0.105 M Ammonium chloride	Yes	8.94	8.17	0.51
Imidazole H7	0.42 M Imidazole hydrochloride	Yes	6.96	7.36	0.17
Imidazole L7	0.025 M Imidazole hydrochloride	Yes	6.87	7.15	0.048
Imidazole 9	0.105 M Imidazole hydrochloride	Yes	8.67	7.85	0.96
Ammonia 1	0.105 M Ammonium chloride	No	9.00	7.46	0.68
Ammonia 2	0.105 M Ammonium chloride, pH set before Mg^{2+} addition	No	6.60	7.57	0.011
Ammonia 3	0.105 M Ammonium chloride	No	7.69	6.92	0.25
Researcher 1	0.42 M urea	Yes	8.21	8.99	0.98
Researcher 2	0.42 M urea	Yes	8.31	8.75	1.75

[a] Synthesis procedure adopted from Besselink et al. (2020).

S 2 Supporting experimental data

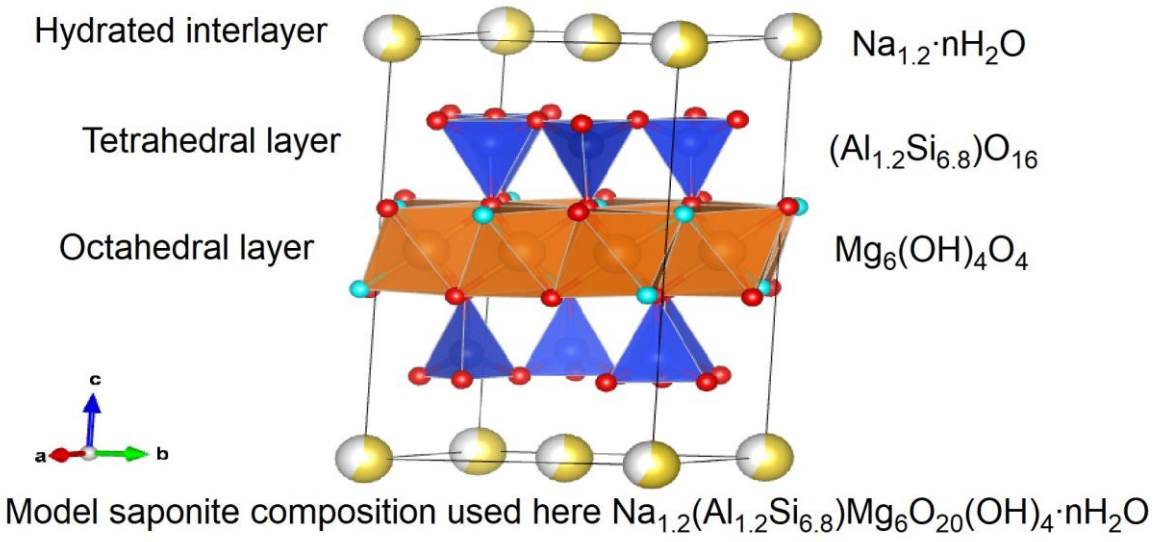

Figure S1. A polygon representation of an ideal unit cell of saponite (modelled using VESTA 3[2]). A solid solution between Al^{3+} and Si^{4+} exists in the tetrahedral layers. In realistic systems a limited solid solution also exists in the octahedral layer between Mg^{2+} and Al^{3+}.

S 2.1 Relative crystallinity and pH of kinetically monitored reactions

Below the relative crystallinities (Figure S2) and pH changes (Figure S3) of all kinetics monitored saponite syntheses experiments are shown. A general trend of decreasing pH in the syntheses where saponite of relative crystallinity of at least 0.3 was obtained could be observed.

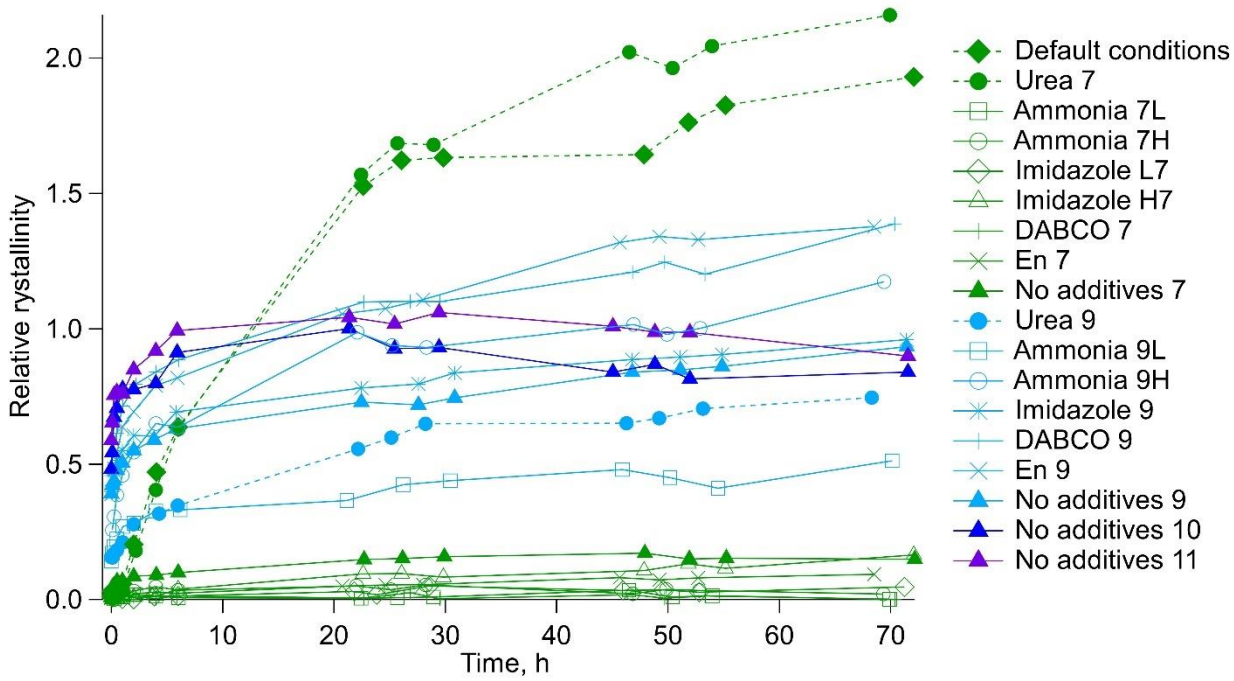

Figure S2. Relative crystallinity changes of kinetics monitored reactions. Green labelled reactions were started at pH ≈ 7, light blue at pH ≈ 9, dark blue at pH ≈ 10, purple at pH ≈ 11 (see Table S1 for exact pH values). Dashed lines indicate reactions containing urea. Reactions that were started at low initial pH, in general produced low crystallinity saponite, unless urea was added.

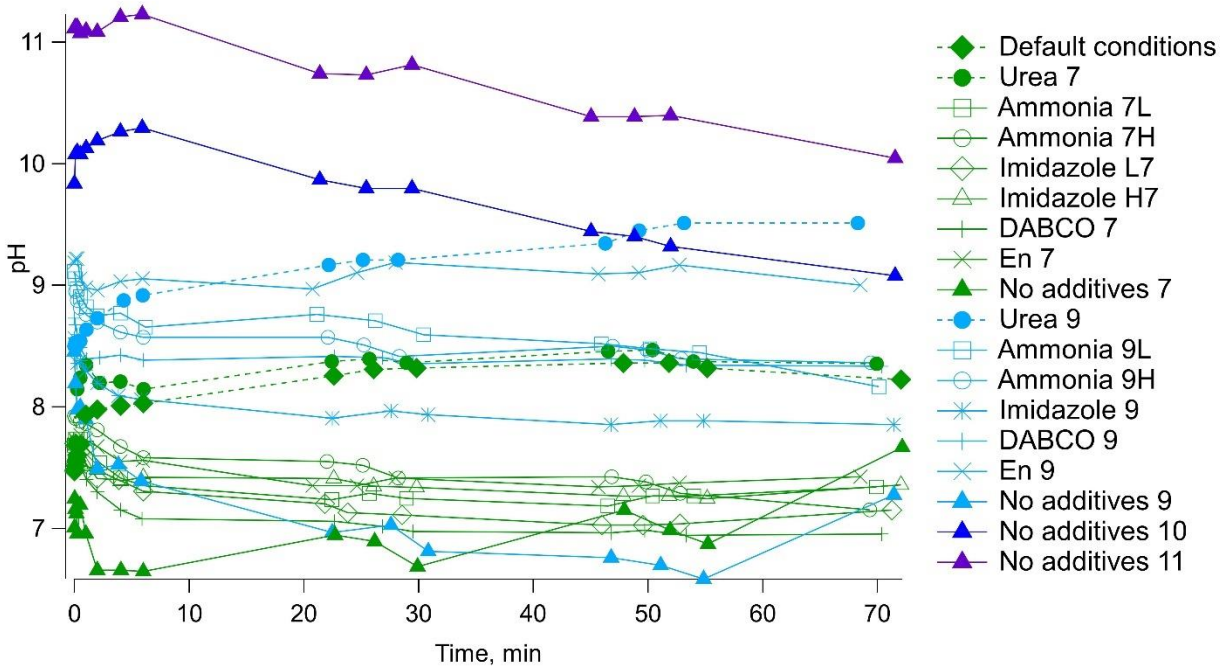

Figure S3. pH change over time of the kinetics monitored reactions. Green labelled reactions were started at pH ≈ 7, light blue at pH ≈ 9, dark blue at pH ≈ 10, purple at pH ≈ 11 (see Table S1 for exact pH values). Dashed lines indicate reactions containing urea. The pH generally decreases during all reactions, with the exception of reactions where urea was used as an additive.

S 2.2 Supporting TEM data

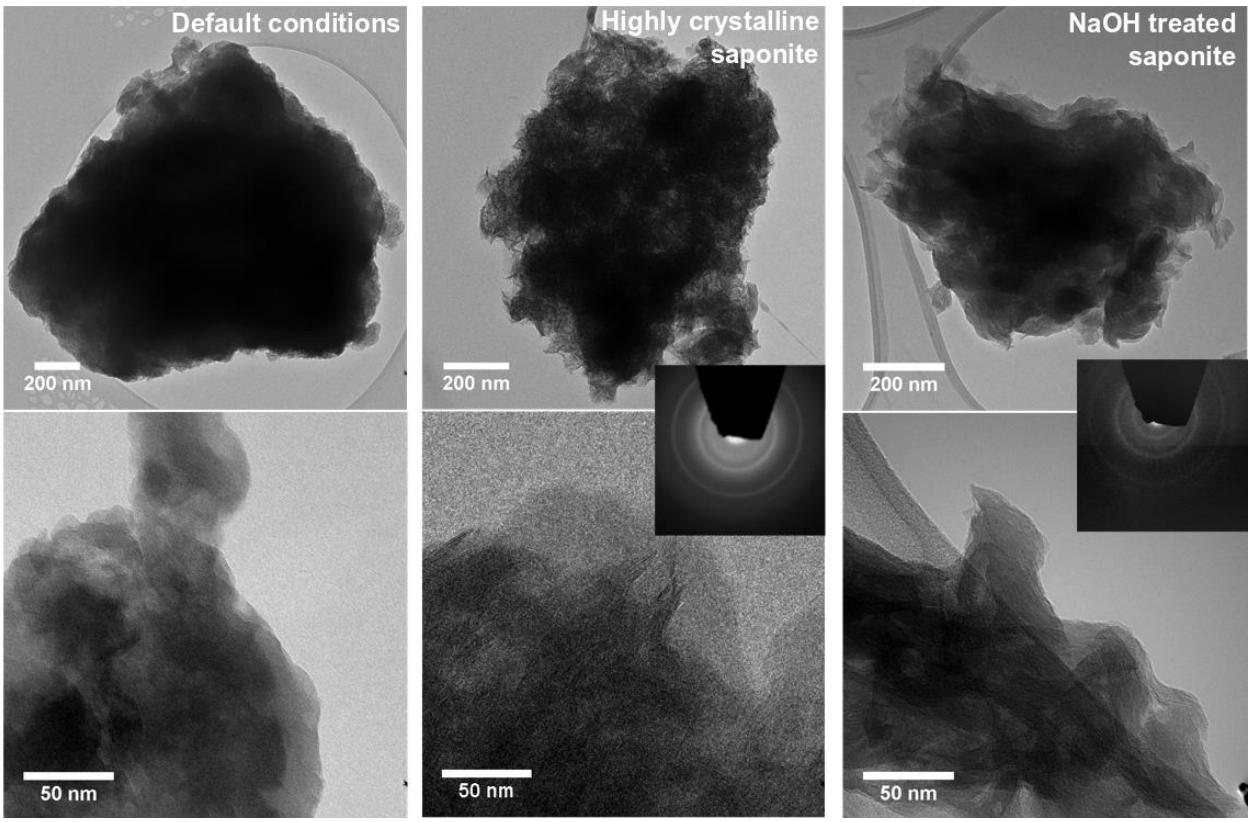

Figure S4. TEM images comparing "default conditions" (left), highly crystalline saponite (center) and NaOH treated saponite (right). Bottom row shows higher resolution images indicating that saponite sheets appear less dispersed in the alkali treated saponite compared to the highly crystalline saponite (from which it was made). Selected area electron diffraction patterns are shown in the insets and are consistent with the XRD data.

Highly crystalline saponite exhibited 5±2 stacked sheets of about 35±5 nm in length (estimate based on observations of over 73 stacked sheets analysed in 24 different TEM images). On the contrary, alkali treated saponite exhibited 8±2 stacked sheets of about 50±20 nm in length (here 6 stacks of sheets were analysed from 3 different TEM images).

S 2.3 Supporting LC-STEM data

A commercially available TEM liquid cell from Protochips Inc. consisting of two silicon E-chips assembled on a Protochips sample holder was used for the in-situ observations of the highly crystalline saponite product in the final reaction mixture. Each E-chip had a 550 µm x 50 µm electron transparent window covered with a 50-nm-thick amorphous silicon nitride film. A 2-µl drop of the highly crystalline saponite suspension was deposited onto the first E-chip. The second E-chip was then placed over the 150 nm gold spacer of the former with their windows in a cross-configuration. The drop of the suspension was hence confined between the two E-chips in a volume defined by the thickness of the gold spacer. The lid of the holder tip resulting in a vacuum-sealed liquid cell then closed the entire chamber. Vacuum check was performed prior to observation in the TEM. The electron flux was calculated by dividing the beam current by the surface area irradiated by the beam. Because of the outward bowing of the SiN membranes under vacuum, the liquid thickness was not homogeneous in the liquid cell and was estimated to be between 250 and 500 nm with 150 nm gold spacer[3]. The presence of aqueous solution around the imaged solids was confirmed by oxygen signal seen in the EDS spectra of the liquid cell in the surrounding medium (Figure S5, black spectrum). The EDS spectrum of the saponite particles (Figure S5, grey spectrum) showed only very minor Mg and Al signals most probably due to strong signal from the O and Si from the thick layer of water and the SiN electron transparent membrane (however, see dry TEM EDS spectra Figure S6 below). The particles in their native environment (aqueous synthesis solution) were composed of aggregates 1000-500 nm in size, very similar to what was observed in conventionally prepared (Figure 2 main document and Figure S4) dry TEM samples. The LC-STEM images suggest that aggregation of

clay sheets is an intrinsic feature of the saponite when synthesised as described in this study and are not an artefact of TEM sample preparation or analyses.

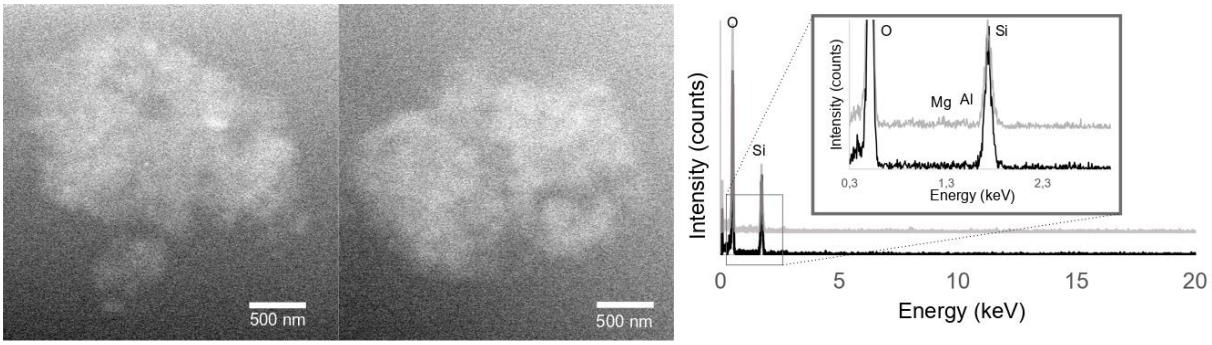

Figure S5. LC-STEM images of two different particles of highly crystalline saponite after 72-hour reaction imaged in their native synthesis solution. The images were acquired with a continuous electron dose rate of 23.46 e^{-} $Å^{-2}$ s^{-1}. EDS spectra of the surrounding medium (black) and of the particle (grey) are shown on the right.

S 2.4 Supporting conventional TEM-EDS data

TEM-EDS spectroscopy was performed of the saponite precursor and compared to the highly crystalline saponite to confirm the magnesium rich nature of the saponite precursor relative to the highly crystalline saponite (Figure S6). The data confirms that both phases contain the elements required for saponite formation, however, the proportion of Mg and Na is higher and the proportion of Al is lower in the saponite precursor compared to the highly crystalline saponite.

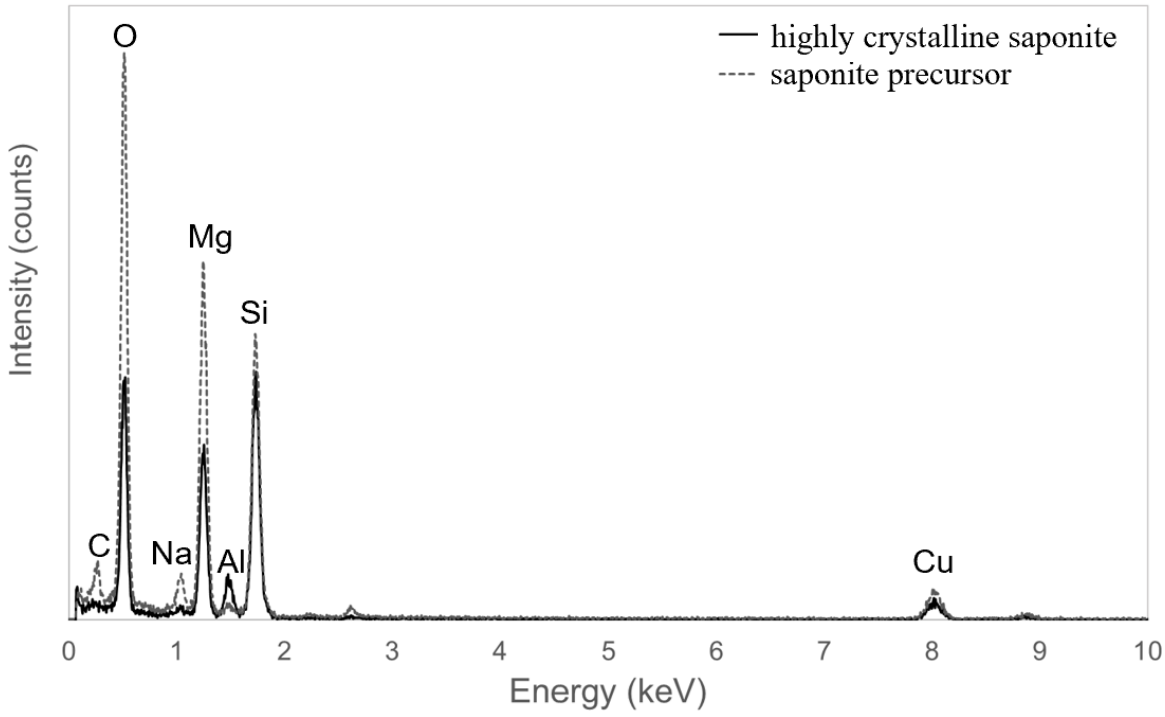

Figure S6. TEM-EDS spectra of the highly crystalline saponite and saponite precursor.

S 2.5 Supporting G(r) data sets

The G(r)s of the alkali treated saponite is very similar to that of the highly crystalline saponite (Figure S7), indicating this treatment did not significantly affect the short-range ordering within the sheets. The G(r) of the aluminosilicate gel starting material (after step 1 of the synthesis, before the addition of Mg^{2+}) is characterized by correlation peaks that decay to noise levels over a shorter distance than 10 $Å^{-1}$. Correlation peaks of the saponite precursor do not decay as rapidly as in the aluminosilicate gel, indicating the degree of short-range order is higher in the saponite precursor compared to the aluminosilicate gel. This is consistent with the interpretation that the saponite precursor consists of saponite nuclei that are nanocrystalline and that contain the short-range structural information of saponite.

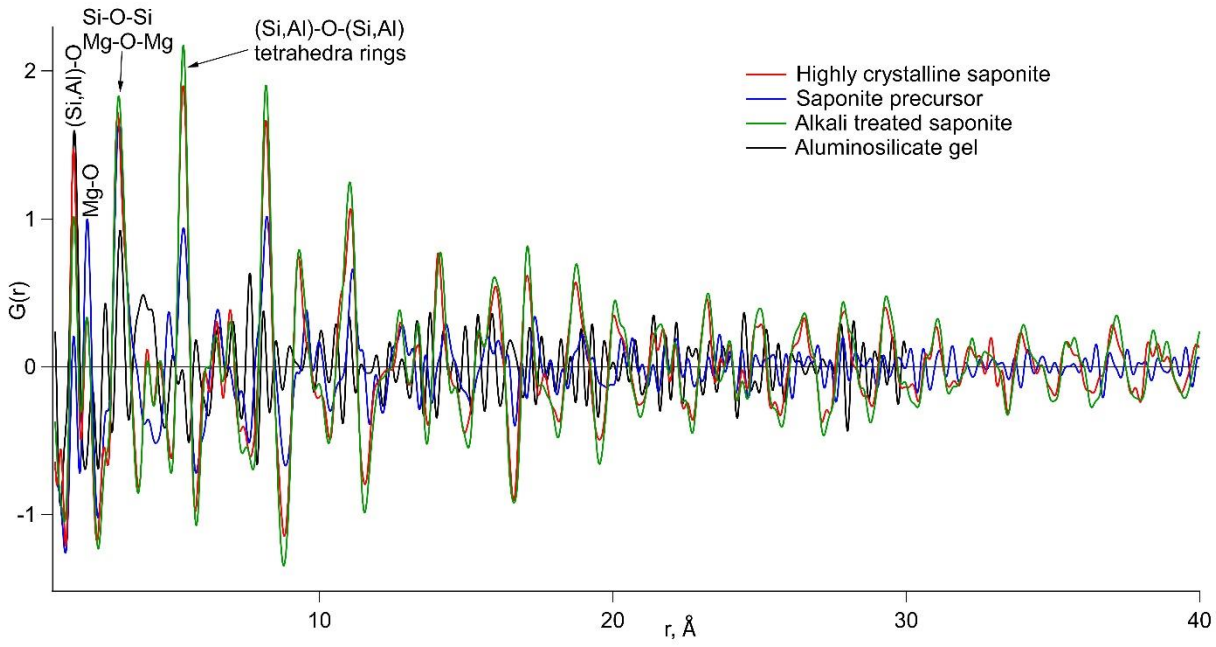

Figure S7. G(r)s of Highly crystalline saponite (red), saponite precursor (blue), alkali treated saponite (green) and aluminosilicate gel starting material (black).

S 2.6 Supporting infrared spectroscopy (IR) data

The ATR-IR spectra shown in Figure S8 are presented without corrections and therefore may not match the exact peak intensity and wavenumber values measured in transmission from other studies[4,5].

There is a certain level of ambiguity in the assignment of IR absorption peaks in the region below 900 cm^{-1} of saponite and other sheet silicates. The biggest disagreement surrounds the interpretation of the peak at 660 cm^{-1} of saponite, here referred to as Mg-OH bending mode. Depending on the literature source and interpretation, this band could also be assigned to Si-O-Si bending [6,7], a vibration of silica tetrahedra rings [7] or a combination of these. Considering the

high number of probable vibrations that could be present in this region perhaps this peak cannot be conclusively assigned without detailed theoretical calculations. Since the aim of this study was not to provide a very accurate IR spectra interpretation, peak assignments from available literature sources was used [5,8–10].

The IR spectra change with reaction time (Figure S8), however, the changes are subtle. The most noticeable change, is the development of a Mg-OH bending mode peak at 660 cm^{-1}, which appears over the course of the first 20-24 hours of the reaction. The other main bands are those representing the asymmetric stretching vibrations of silicon or aluminium in tetrahedral geometry (aluminosilicate tetrahedra) at ~ 1000 cm^{-1}, as well as the broad OH stretching band at ~ 3000-3500 cm^{-1} corresponding to water in the clay sheet interlayer and the adsorbed water. Water also gives rise to a peak corresponding to the water bending mode at 1640 cm^{-1}. There are multiple peaks between 800 cm^{-1} and 550 cm^{-1} that correspond to various bending modes of the aluminosilicate tetrahedra in the amorphous precursor. The partially visible band at about 490 cm^{-1} corresponds to Mg-O stretching and the Si-O-Si moiety oxygen atom rocking mode. A more subtle feature is the peak at 3677 cm^{-1} that appears towards the end of the reaction and corresponds to the O-H bond stretching vibration in the MgO(OH) layer.

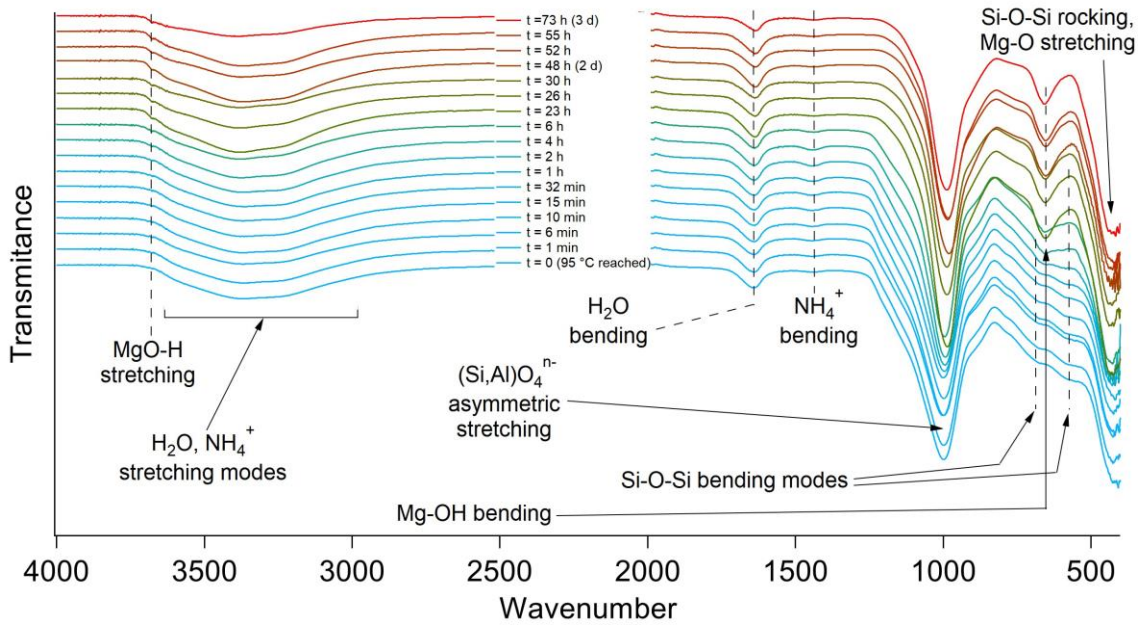

Figure S8. Time series of IR spectra of the solids from the reaction aliquots and the final product from the "Default conditions" (Tables 1, S1).

As the IR spectra were visually very similar and because there were no new, non-overlapping or easily-fittable peaks changing during the time course of the reaction, principal component analysis (PCA) was used to evaluate the IR data and compare it with the changes observed in the XRD data (Figure 4 main document). The analyses revealed that the biggest change was displayed by the second principal component (PC2, Figure S9). This figure exemplifies the progress of the "Default conditions" synthesis reaction and demonstrates a very good agreement between the relative crystallinities derived from the XRD patterns and the IR-PCA PC2. However, no clear trend in the IR-PCA scores was observed during the development of the very poorly crystalline saponite, despite the fact that the relative crystallinity still showed a clear trend that appeared to match qualitative visual observations of the changes in the XRD

patterns (Figure 4, main document). This supports the decision to use the relative crystallinity as the primary measure by which the reaction progress was evaluated.

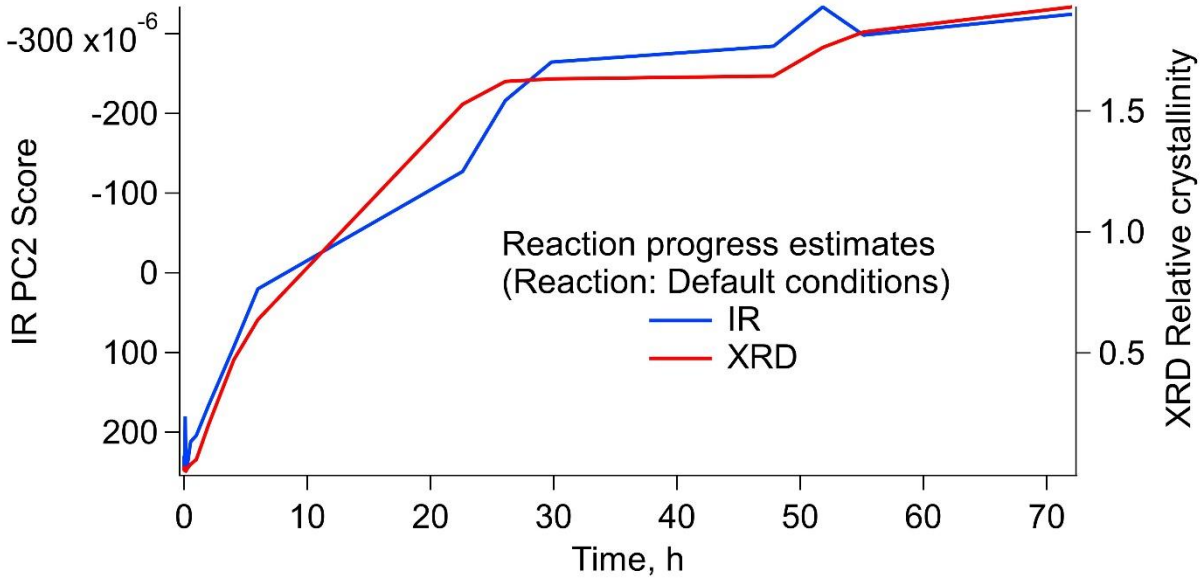

Figure S9. Comparison of relative crystallinities calculated from the XRD patterns and the 2nd principal component (PC2) score of the PCA of the IR spectra from the kinetically monitored saponite synthesis experiment "Default conditions".

S 2.7 Supporting data from saponite synthesis experiments at low concentrations

To investigate concentration effects on the reaction products, the reaction procedure of the synthesis "Default conditions" was modified by changing the amount of water added in the dilution steps. In these experiments (Figure S10) adequate amounts of water were added to both, the gel after the 1h heating step and to the Mg^{2+} containing solution to achieve the desired degree of dilution. For example, a concentration of 1 in Figure S10 corresponds to that

used in “Default conditions”. To achieve concentration of 0.5, both the aluminosilicate gel and Mg^{2+} solutions were diluted two times. Few reactions (purple crosses Figure S10) were performed with double the concentration of aluminosilicate gel relative to the magnesium chloride added (total reaction concentration measured with respect to Mg^{2+}).

The data shows that the relative crystallinities of the reaction products (after 3-day synthesis) did not show any conclusive trend in terms of crystallinity change (Figure S10). The biggest change in relative crystallinity occurs during the first 12 hours of the reaction, although the reactions involving urea showed slower changes. Here however, only the final product (after 72 hours) was monitored. Considering the maximal dilution factor was 40 (0.00521 M instead of 0.21 M Mg^{2+}) and that the reaction takes minimum of ≈10 h to reach effective completion, it is inconceivable that the reaction product’s crystallinity would not be adversely affected if the overall saponite formation rate would be limited by a purely dissolved species (Mg^{2+}, urea, imidazole). This confirms the reaction rate is controlled by the dissolved aluminosilicate gel, even at a dilution factor of 40. This further suggests, the reaction mixture is still saturated with respect to the aluminosilicate gel and implies that only the concentration of $Mg^{2+}_{(aq)}$ was changed by the dilution. This confirms Mg^{2+} is not involved in the rate determining step as has been reported before[1]. The effective concentration of the rate limiting component (aluminosilicate gel) was not changed, in agreement with the reaction mechanism interpretation provided in the main text.

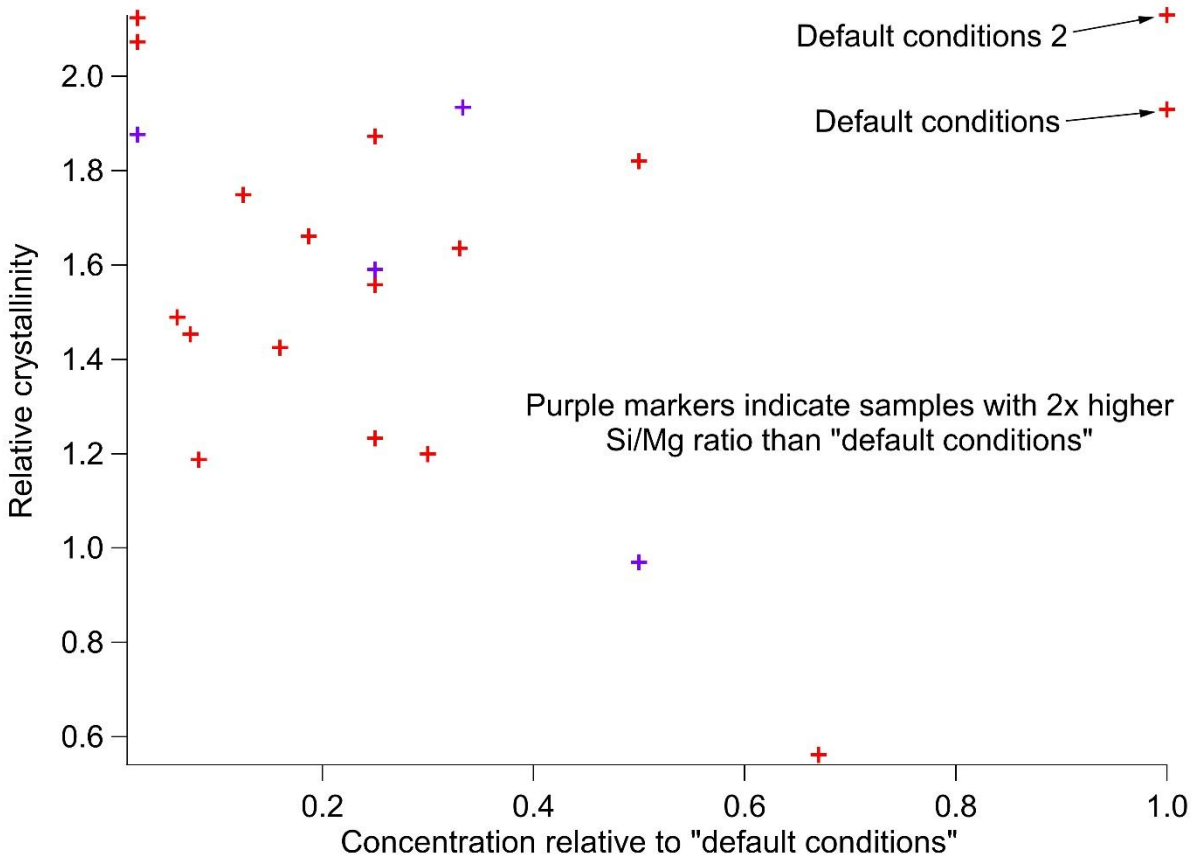

Figure S10. Relative crystallinity of the saponite formed after three days versus the concentration of the reaction mixture relative to the "Default conditions" and a repeat experiment "Default conditions 2" (see description above and Table S1).

S 3 Additional modelling data

S 3.1 Thermodynamic modelling

The thermodynamic modelling calculations show the reaction mixture was highly oversaturated with respect to saponite. Brucite is comparatively a lot more soluble than saponite, however, based on the calculations it is also supersaturated under the reaction

conditions. The calculations indicate that under the reaction conditions employed in this study brucite precipitation should occur when the pH exceeds about 7.6.

Table S2. Saturation indexes (SI) computed of the available variations of saponite and brucite mineral phases at various pH and temperature from Geochemical Workbench implemented with thermo.tdat database.

Mineral phase	SI (20 °C, pH 13)	SI (20 °C, pH 9.8)	SI (100 °C, pH 13)	SI (100 °C, pH 7.6)
Saponite-Na	23.3	23.8	16.8	23.1
Saponite-Mg	22.9	23.8	16.5	23.6
Saponite-H	20.3	21.9	13.9	21.9
Brucite	4.9	1.0	6.6	1.0

S 3.2 Kinetic modelling discussion

An intrinsic problem in studying the formation kinetics of saponite or any other clay minerals is the difficulty in defining what the product of the reaction is at any point in time. Saponite as a mineral is defined by both, its chemical composition as well as its structure, yet perfectly crystalline saponite has so far not been obtained in a laboratory synthesis. Furthermore, the experimental data obtained in this study and by other authors [1,11] implies the saponite structure follows a continuous evolution with increasing crystallinity. This makes it difficult to quantify how far a reaction has progressed from the starting materials to the 'final' crystalline saponite product. Reactions that produce a low crystallinity saponite (most of the ones started at about pH 7) often did not show discernable (110) and (020) peaks. This indicates that the final products obtained in these reactions was not the same as the more crystalline final

product obtained in the reactions started at a higher pH. Therefore, the reactions cannot be directly compared as neither the reaction conditions nor the products were the same.

Another set of difficulties encountered in modelling the reaction progress was the change in reaction conditions, namely the variations in pH. OH^- is stoichiometrically involved in saponite formation as a reagent as well as a catalyst as it helps in achieving the dynamic equilibrium between the aqueous and solid components of the aluminosilicate gel. However, as can be seen in Figure S3, the reaction pH variations during the reactions were not smooth and systematic and cannot be described with a simple equation. Finally, despite the results from this and the previous studies that followed saponite formation processes[1,12–14], the elementary steps involved in the saponite growth are still poorly understood. Combined with the fact that the starting aluminosilicate gel cannot be considered a single chemical species as its reactivity is certainly non-uniform[15–18], the derivation of an accurate model describing the formation of saponite is highly challenging.

Therefore, it is not surprising that depending on the metric chosen to monitor the reaction progress, different results can be obtained. To demonstrate this, the G(r) atom pair correlation peaks measured and used to monitor the reaction progress by Besselink et al. (2020) have been plotted and compared to the relative crystallinity of our solid from a reaction performed the same way (Default conditions, Tables a, S1). Besselink et al. (2020) describes the saponite formation as a 1^{st} order process and their data shows a reasonably good fit to this model. However, a 0^{th} order process can also be fit to the same data, with the quality of the fit being very similar to that of a 1^{st} order fit. Furthermore, both, 1^{st} and 0^{th} order fits were

mathematically more appropriate to Na-O bond intensity data compared to Mg-O or Si-Oct-Si intensity data (all derived from G(r)[1]), see figure S11.

However, the biggest problem encountered in previous saponite synthesis studies is a misunderstanding of the role of reagents and additives used. In Besselink et al. (2020) the OH^- that is required for saponite formation was produced by the decomposition of urea. Therefore, the formation rate of saponite is limited by the rate of urea decomposition. Urea decomposes in aqueous solution following a 1st order rate law with an activation energy between 83 and 130 kJ/mol[19,20]. The activation energy of saponite formation has been determined[1] to be 100±9 kJ/mol, which is close to the middle of the range of the reported activation energies of urea decomposition. Therefore, the usefulness of urea as an additive to study saponite formation becomes questionable as it is impossible to distinguish if the activation energy and the reaction progression trends measured are those of saponite formation or just those for urea decomposition.

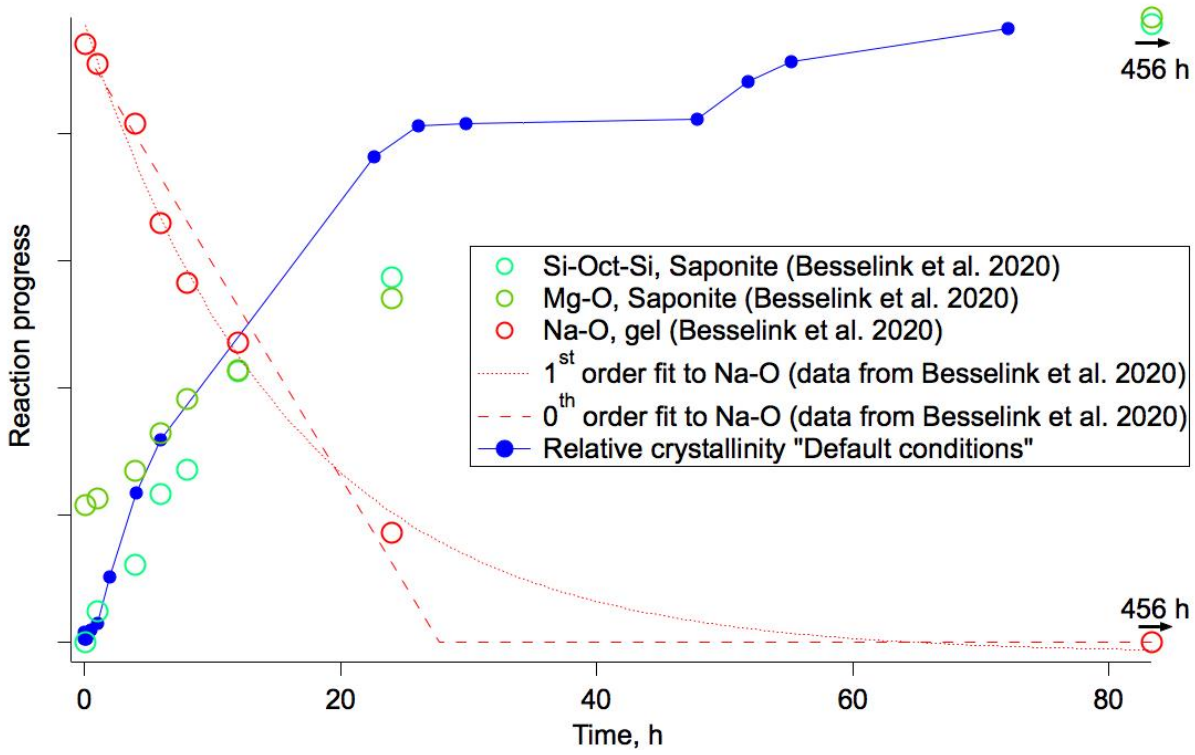

Figure S11. Reaction progress monitoring data derived from G(r) analysis by Besselink et al. (2020). 1st and 0th order reaction fits to the Na-O distances to the Na-O distance data by Besselink et al. (2020) are shown. Also added is the relative crystallinity of "Default conditions", effectively a replicate of the reaction performed by Besselink et al. (2020).

S 4. Additional information of the XRD data were processing and analysis

Cu-XRD patterns were measured both, with the samples in the sample holder, as well as of the empty sample holder (background). The sample holder consists of two 20 µm thick acetate films between which the sample is supported. The majority of background counts were caused by air scattering, not the acetate films. The intensity adjusted background scattering patterns

were subtracted from the sample scattering patterns. The background intensity was adjusted such that in the Q region Q = 0.8 – 1 $Å^{-1}$ after the background subtraction, the lowest intensity value of the sample scattering pattern became zero.

Due to the very poor crystallinity of even the most crystalline saponite samples any form of Rietveld refinement or other well-established quantitative analyses of crystalline samples were not possible. Therefore, an empirical crystallinity determination method was devised. To calculate the relative crystallinity, the background subtracted patterns were first boxcar smoothed with a 3 degree 2*Θ wide filter. The relative crystallinity was then calculated from the ratio between the maximum value in Q range Q = 2.35 – 2.70 $Å^{-1}$ and the minimum value in the Q range Q = 2.05 – 2.35 $Å^{-1}$ (Figure S12) according to the following equation:

$$Relative\ crystallinity = \frac{Max.value(Q = (2.35; 2.70))}{Min.value(Q = (2.05; 2.35))} - 1 \quad eq.S1$$

The relative crystallinity scales from 0 (fully amorphous) to in principle unlimited value although in this study the highest relative crystallinity calculated was 2.77 for the alkali treated saponite.

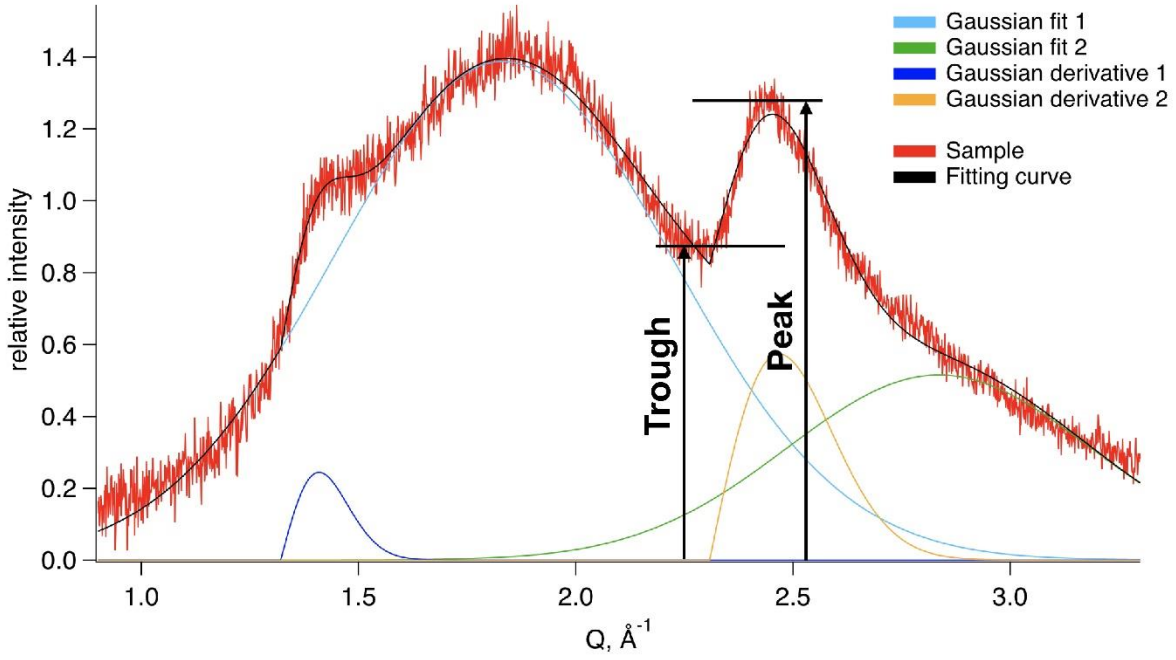

Figure S12. Cropped XRD scattering pattern from a typical medium-crystallinity saponite sample showing how the relative crystallinity could be empirically calculated by dividing "Peak = maximum" and "Trough = minimum" of a peak. An attempt of a peak fitting using Gaussian and Gaussian derivative functions is also shown. For this particular sample this fitting described the pattern rather well, but such fits were not universally applicable to all samples.

This, empirical, assessment of the saponite crystallinity (Figure S12 eq. S1) was chosen as the best approach to assess saponite crystallinity because it was the most self-consistent (Figure S9, S12). Peak fitting of the saponite and the amorphous precursor produced mathematically satisfactory descriptions of the patterns, however, the quantification data was inconsistent across different reaction series and even samples within the same series. One possibility considered variations in the amount of sample used in each diffraction experiment as the

measurements were performed in a flat plate geometry. A highly consistent sample preparation procedure did not resolve this, presumably due to different porosities of the dried samples (see further information below sec. S 5.2). This was indirectly hinted at by the low density of the saponite product obtained and the difficulties of observing significant scattering signals from the saponite products when analyzed in a 0.5 mm diameter capillary. Normalization of the scattering intensities also proved troublesome due to some peaks being very broad and there being no Q regions in the Cu-XRD patterns that would be totally unaffected by nearby scattering peaks that could be considered pure background. The main cause in difficulty applying peak fitting methods to the Cu-XRD pattern analysis was, however, the complex shape of the saponite scattering peaks that could not be accurately described by simple functions, and good theoretical description of these peak shapes was not available.

S 5 Additional points of discussion

S 5.1 The effect of additives on saponite synthesis

It was found that organic additives or added bases have no significant effect on the reaction progress or outcome when two reactions, differing only by the added organic compound or its concentration, were compared (Figures S2, S3). This implies that coordination or chelation of metal ions (Mg^{2+}, Al^{3+}) do not change the rate limiting step of the reaction. Any templating effects are also therefore insignificant and no notable differences between reaction products of reactions featuring different or no additives where observed besides those that could be correlated to different pH. It was found that the initial reaction rate was higher in reaction "Urea 7" compared to "Default conditions". These two reactions differed only by the addition

of an imidazole hydrochloride buffer to the reaction “Default conditions”. This difference exists because the “buffer” acts as a weak acid and consumes OH^- ions formed by hydrolysis of ammonia as the urea decomposes. This slows down the beginning of the reaction by keeping the pH low. However, the imidazole hydrochloride is consumed during the first hour of the reaction and from that point onwards the reaction proceeds similarly as in its absence. The addition of a weak acid, like imidazole hydrochloride or similar, delays the growth of saponite sufficiently long that the reaction mixture can be heated to the reaction temperature of 95 °C before the reaction actually begins. This effect only works if urea is used as an OH^- source. This approach was used by Besselink et al. (2020) who used histidine hydrochloride as a buffer. The low histidine hydrochloride concentration relative to that of urea (3.5 mmol of histidine hydrochloride vs 42 mmol of urea), negated the effect of the first few mmol of urea decomposing. If NaOH is used to achieve the desired initial pH, the weak acid is instantaneously consumed as acid-base proton exchange is one of the fastest reactions in an aqueous solution. This makes such additives unnecessary. The use of urea as an additive obscures the true reaction progression (see sec S 3.2 above).

S 5.2 Discussion of experimental errors and error analysis

Random errors in the relative crystallinity evaluation were estimated to be no more than ±10 %. Random errors in each pH measurement were estimated to be no larger than ±0.2 pH units. Both were estimated by observing variations in the relative crystallinity and pH variations (Figures S2, S3) and assuming the variations of both parameters should be smooth. The errors were considered to be 150 % of the largest observed deviation from a smooth trend.

The conditions at which the aluminosilicate gel synthesis was performed (Supporting information 1.2 step 1) were highly alkaline. After dilution with water, before the Mg^{2+} solution addition, the pH was ≈12.6. At such highly alkaline conditions at 100 °C, the glass of the reaction vessels (borosilicate glass 3-necked round bottom flasks) can slowly dissolve and be incorporated into the reaction mixture. This was indeed observed as after prolonged and repeated use the glass gained a corroded appearance. The dissolved glass contributes to the final saponite material as it slightly alters the Si:Al ratio (intended to be 6.8:1.2). Despite the fact that the overall composition of the final saponite could be slightly affected this change in Si:Al ratios, this does not impact the overall formation mechanism of saponite.

There are some experimental parameters that are extremely difficult, if not impossible, to quantify. One of the most important ones here is the reagent mixing rate. This is important as the saponite nucleation is very rapid and this significantly impacts the crystallinity of the final product. A significant source of uncertainty was the control over the homogeneity of the aluminosilicate gel. This gel was a suspension (settles on a timescale of tens of minutes). However, during the 1 h reaction time under reflux, it often developed a ring of a solid material around the glass-water-air interface. It is unknown if this seemingly denser agglomeration of solid had the same properties as the solid gel particles in suspension. The segregation of this material seemed to be affected by the stirring rate and the size of the flask relative to the volume of the liquid. Slower stirring rates and higher liquid volume fractions minimized, though not eliminated, this phase segregation.

Furthermore, considering the heterogeneous nature of the aluminosilicate gel, the rate and extent at which any added chemicals (Mg^{2+}, urea, organic additives) equilibrates with the gel

particles cannot be estimated. An indication that equilibration with the suspension may be a problem was indicated by a very slow rate at which the pH equilibrated, when setting the reaction's starting pH with HCl or NaOH, which is very atypical for a simple acid-base exchange.

The random uncertainties in each experiment were tested by two replicate experiments of the "Urea 9" experiment (Table S1). These two experiments were performed at the same time by two different researchers using the same reagent stock solutions (Figures S13, S14 and S15). Although the initial pH was set at room temperature to within 0.02 pH units of the desired value of pH 9, after heating to reaction temperature of 95 °C the first aliquot (1st data point) had pH values of 8.21, 8.31 and 8.85 for researcher 2, researcher 1 and "Urea 9" respectively. This variation it is the likely source of the discrepancy in the final relative crystallinities of 0.75, 0.98 and 1.75 for the "Urea 9", researcher 1 and researcher 2 respectively. This follows the expected trend of higher final relative crystallinity resulting from lower initial pH if urea is added to the reaction mixture. However, the causes behind such different pH evolution during heating of a very similar reaction setup from room to reaction temperature over a very similar time interval were not discovered.

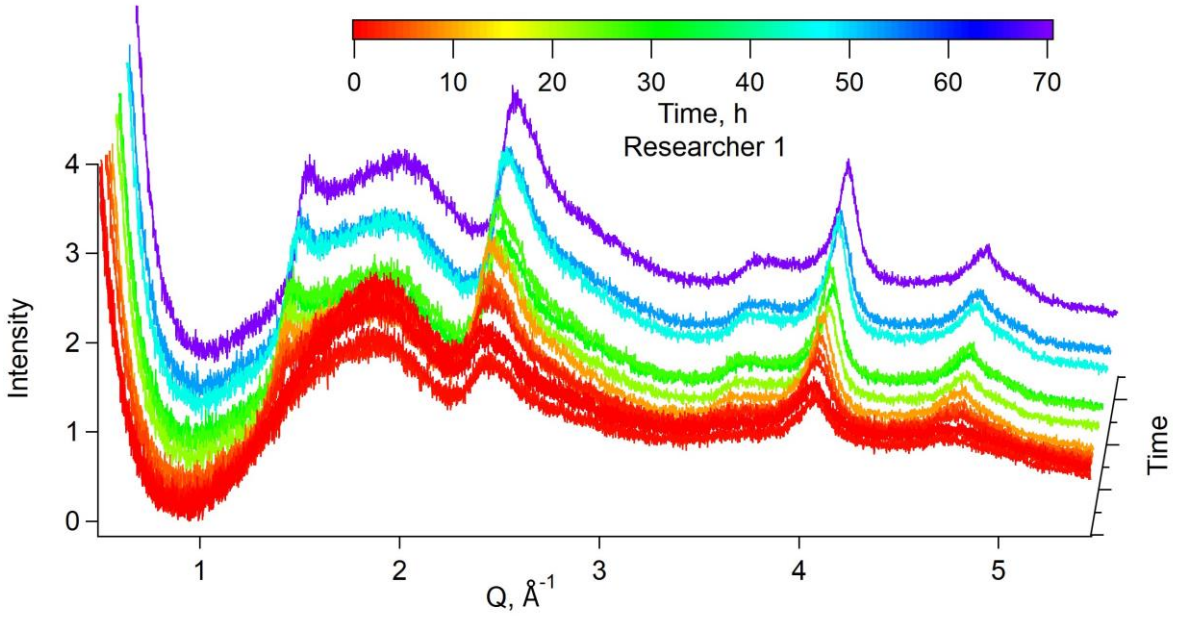

Figure S13. Cu-XRD patterns of saponite synthesis (replicate of "Urea 9") time series performed by Researcher 1

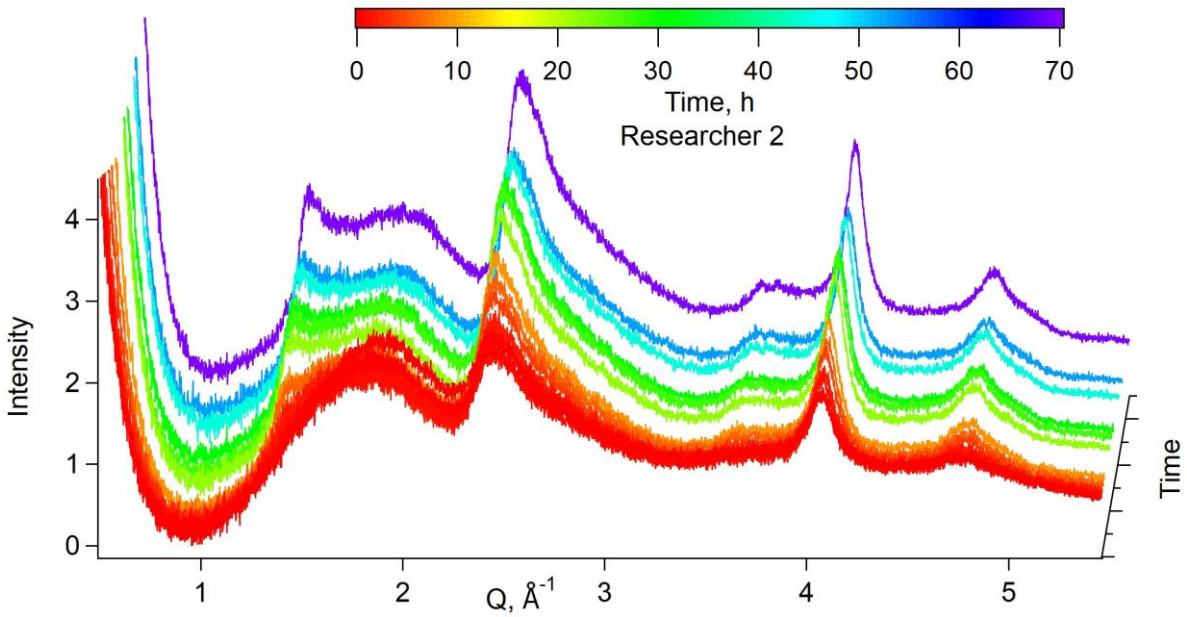

Figure S14. Cu-XRD patterns of saponite synthesis (replicate of "Urea 9") time series performed by Researcher 2.

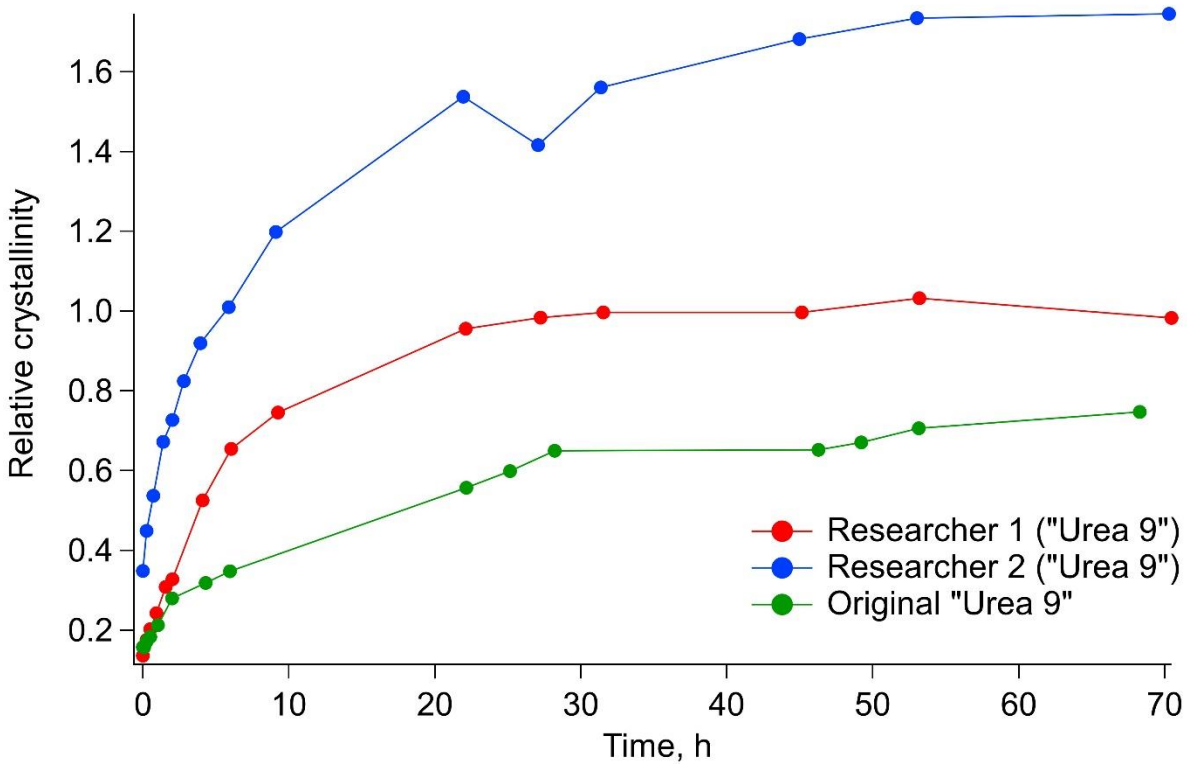

Figure S15. Relative crystallinity of two replicates of "Urea 9" performed by two Researchers working side by side in the same lab performing the same reaction and using the same reagents. The replicate date is compared to the original reaction "Urea 9".

The macroscale properties of the saponite samples were not fully understood during this study. The yield of the solid material obtained after the drying of the centrifuged and washed material was always about 100% if the ideal formula $Na_{1.2}(Al_{1.2}Si_{6.8})Mg_6O_{20}(OH)_{4\ (s)}$ was used. Due to the variable hydration water content in the formed saponite, the mass obtained was always higher than the ideal formula mass of saponite. However, the volume of the mortar ground powder differed significantly between different syntheses with no clear pattern. It was

observed though that the product of high relative crystallinity was much easier to grind and turn into a powder using a mortar and pestle compared to the syntheses that yielded low relative crystallinity saponite or a pure aluminosilicate gel. However, the alkali treated saponite was the most difficult sample to grind and resembled glass. The controls of these mechanical properties of the samples were not understood.

6 References

(1) Besselink, R.; Stawski, T. M.; Freeman, H. M.; Hövelmann, J.; Tobler, D. J.; Benning, L. G. Mechanism of Saponite Crystallization from a Rapidly Formed Amorphous Intermediate. *Cryst. Growth Des.* **2020**, *20*, 3365–3373. https://doi.org/10.1021/acs.cgd.0c00151.

(2) Momma, K.; Izumi, F. VESTA 3 for Three-Dimensional Visualization of Crystal, Volumetric and Morphology Data. *J. Appl. Crystallogr.* **2011**, *44* (6), 1272–1276. https://doi.org/10.1107/S0021889811038970.

(3) Piffoux, M.; Ahmad, N.; Nelayah, J.; Wilhelm, C.; Silva, A.; Gazeau, F.; Alloyeau, D. Monitoring the Dynamics of Cell-Derived Extracellular Vesicles at the Nanoscale by Liquid-Cell Transmission Electron Microscopy. *Nanoscale* **2018**, *10* (3), 1234–1244. https://doi.org/10.1039/c7nr07576f.

(4) Kloprogge, J. T.; Breukelaar, J.; Jansen, J. B. H.; Geus, J. W. Development of Ammonium-Saponites from Gels with Variable Ammonium Concentration and Water Content at Low Temperatures. *Clays Clay Miner.* **1993**, *41* (1), 103–110. https://doi.org/10.1346/CCMN.1993.0410111.

(5) Farmer, V. C. Infrared Spectra of Minerals. Mineralogical Society 1974.

(6) Sugat, K.; Rusling, J. F. Structural Characterization of Surfactant and Clay-Surfactant Films of Micrometer Thickness by FT-IR Spectroscopy. *Langmuir* **1993**, *9*, 3649–3655. https://doi.org/10.1021/la00036a048.

(7) Handke, M.; Mozgawa, W. Vibrational Spectroscopy of the Amorphous Silicates. *Vib. Spectrosc.* **1993**, *5* (1), 75–84. https://doi.org/10.1016/0924-2031(93)87057-Z.

(8) Kloprogge, J. T.; Frost, R. L. The Effect of Synthesis Temperature on the FT-Raman and FT-IR Spectra of Saponites. *Vib. Spectrosc.* **2000**, *23* (1), 119–127. https://doi.org/10.1016/s0924-2031(00)00056-4.

(9) Madejová, J. FTIR Techniques in Clay Mineral Studies. *Vib. Spectrosc.* **2003**, *31* (1), 1–10. https://doi.org/10.1016/S0924-2031(02)00065-6.

(10) Taylor, W. R. Application of Infrared Spectroscopy to Studies of Silicate Glass Structure: Examples from the Melilite Glasses and the Systems Na2O-SiO2 and Na2O-Al2O3-SiO2. *Proc. Indian Acad. Sci. - Earth Planet. Sci.* **1990**, *99* (1), 99–117. https://doi.org/10.1007/BF02871899.

(11) Vogels, R. J. M. J.; Kloprogge, J. T.; Geus, J. W. Synthesis and Characterization of Saponite Clays. *Am. Mineral.* **2005**, *90* (5–6), 931–944. https://doi.org/10.2138/am.2005.1616.

(12) Decarreau, A. Cristallogenèse Expérimentale Des Smectites Magnésiennes : Hectorite, Stévensite. *Bull. Minéralogie* **1980**, *103* (6), 579–590. https://doi.org/10.3406/bulmi.1980.7423.

(13) Decarreau, A. Etude Expérimentale de La Cristallogenèse Des Smectites. Mesures Des Coefficients de Partage Smectite Trioctaédrique - Solution Aqueuse Pour Les Métaux M2+ de La Première Série de Transition. *Sci. Géologiques, Bull. mémoires* **1983**, *74* (1), 17–23.

(14) Vogels, M. J.; Breukelaar, I. J.; Kloprogge, J. T.; Jansen, J. B. H.; Geus, J. W. Hydrothermal Crystallization of Ammonium-Saponite at 200 ° C and Autogeneous Water Pressure. *Clays Clay Miner.* **1997**, *45* (I), 1–7.

(15) Krznarić, I.; Antonić, T.; Subotic, B. Physical Chemistry of Aluminosilicate Gels. Part 1. Influence of Batch Concentration on Chemical Composition of the Gels. *Zeolites* **1997**, *19* (1), 29–40. https://doi.org/10.1016/S0144-2449(97)00049-3.

(16) Roelofs, F.; Vogelsberger, W. Dissolution Kinetics of Synthetic Amorphous Silica in Biological-like Media and Its Theoretical Description. *J. Phys. Chem. B* **2004**, *108* (31), 11308–11316. https://doi.org/10.1021/jp048767r.

(17) Dent Glasser, L. S.; Lachowski, E. E. Silicate Species in Solution. Part 1. Experimental Observations. *Dalt. Trans.* **1980**, 393–398.

(18) Lesley, B.; Glasser, S. D.; Lachowski, E. E. Silicate Species in Solution. Part 2. The Structure of Polymeric Species. *Dalt. Trans.* **1980**, 399–402.

(19) Shaw, W. H. R.; Bordeaux, J. J. The Decomposition of Urea in Aqueous Media. *J. Am. Chem. Soc.* **1955**, *77* (18), 4729–4733. https://doi.org/10.1021/ja01623a011.

(20) Polino, D.; Parrinello, M. Kinetics of Aqueous Media Reactions via Ab Initio Enhanced

Molecular Dynamics: The Case of Urea Decomposition. *J. Phys. Chem. B* **2019**, *123* (31), 6851–6856. https://doi.org/10.1021/acs.jpcb.9b05271.

$$(Al,Si)\ Gel_{(s)} + OH^- \xrightarrow[\text{Dissolution}]{0^{th}\ \text{order}} 2\ (Al,Si)\ Gel_{(aq)} \xrightarrow[\text{Precipitation}]{2^{nd}\ \text{order}} Saponite_{(s)}$$